Xenosiderophore transporter gene expression and clade-specific filamentation in *Candida auris* killifish infection

Hugh Gifford[a], Tina Bedekovic[a], Nicolas Helmstetter[a], Jack Gregory[a], Qinxi Ma[a], Alexandra C. Brand[a], Duncan Wilson[a], Johanna Rhodes[b,c], Mark Ramsdale[a], Tetsuhiro Kudoh[d,1], Rhys Farrer*[a,1]

Abstract

Candida auris is an emerging infectious agent and World Health Organisation (WHO) critical priority fungal pathogen. Rising drug resistance, massive nosocomial outbreaks and diagnostic challenges complicate clinical treatment, resulting in a patient mortality rate of ~45%. Surprisingly, gene expression profiles of *C. auris* have not yet been described during infection *in vivo*. To understand transcriptional responses during in-host infection, we developed a thermo-relevant fish embryo yolk-sac microinjection model (*Aphanius dispar*; Arabian killifish; AK) that mimics human body temperature. This allowed us to interrogate infection dynamics through dual host-pathogen RNA-seq at 24 and 48 h post injection (HPI) at 37 °C across the five major clades (I-V) of *C. auris*. Host gene expression following infection indicated features of heat shock, complement activation, and nutritional immunity, including haem oxygenase (*HMOX*) expression in response to clade IV infection. We identified an *in vivo* transcriptional signature across five clades of *C. auris* that was highly enriched for putative xenosiderophore transmembrane transporters. We describe this newly-discovered seventeen-member xenosiderophore transporter candidate (*XTC*) family in terms of individual gene expression patterns, and a sub-clade of five putative haem transport-related (*HTR*) genes, also up-regulated during infection. Only the basal clade V isolate formed filaments during infection, coinciding with typical and atypical regulators of

morphogenesis, including *UME6*, *HGC1*, and the novel adhesin *SCF1*. Clades I and IV demonstrated increased virulence, coinciding with up-regulation of three *HTR* genes in clade IV, and the mating-type locus (*MTL*) non-mating gene *PIKA* in both. Our study suggests that *XTC* and *HTR* genes may play a critical role in *C. auris* virulence, making excellent targets for further investigation and potential therapy.

Keywords: *Candida auris*, virulence, gene expression, transcriptome, pathogenicity, Arabian killifish, *Aphanius dispar*, siderophore transport, mating-type locus, filamentation

[a]MRC Center for Medical Mycology, University of Exeter, Geoffrey Pope Building, Stocker Road, Exeter, United Kingdom, EX4 4QD
[b]Department of Medical Microbiology, Radboudumc, Geert Grooteplein Zuid 10, Nijmegen, Netherlands, 6525 GA
[c]MRC Centre for Global Infectious Disease Analysis, Imperial College London South Kensington Campus, London, United Kingdom, SW7 2AZ
[d]Biosciences, University of Exeter, Geoffrey Pope Building, Stocker Road, Exeter, United Kingdom, EX4 4QD
[1]Co-Senior Author
*Corresponding Author - R.Farrer@exeter.ac.uk

Introduction

C. auris is an ascomycetous yeast in the *Metschnikowiaceae* family that has rapidly transitioned from recent emergence to global public health threat[1] and World Health Organisation (WHO) critical priority human fungal pathogen[2]. Despite the oldest known historical isolate dating from 1996[3], the first formal species identification occurred in 2008[4]. Within ten years, *C. auris* had caused nosocomial outbreaks around the world, with high rates of azole antifungal drug resistance and a rising incidence of

pan-drug resistance[5]. These factors required extreme measures including Intensive Care Unit (ICU) shutdowns and massive infection control costs[6–8]. Worryingly, *C. auris* is now a leading cause of invasive candidiasis in several hospital settings globally[9,10]. Distinct clades of *C. auris*, including a sixth clade identified and described in publications only in 2024[11,12], indicate the simultaneous emergence of multiple lineages that are highly adapted for human infection[13,14]. The clinical impact, phenotypic traits and simultaneous emergence of multiple clades of *C. auris* underscore the urgency to understand its mechanisms of pathogenicity.

The factors governing in-host fitness and virulence during infection are poorly understood. *C. auris* bloodstream infection is associated with a crude mortality of ~45%[15]. Virulence factors in other distantly related *Candida* species, such as *C. albicans*, include hypha-mediated invasion[16], the invasin Als3[17], and the secreted toxin, candidalysin[18]. In contrast, *C. auris* has been shown to reproduce as budding yeasts in mammalian tissues[19,20]. Although *C. auris* possesses multiple adhesins associated with an aggregation phenotype[21,22], there has been no evidence of toxin synthesis[23,24]. *C. auris* evades host immune responses through cell surface masking[25], secreted aspartyl protease digestion of host tissue[26], and intra-phagocytic survival with cell lysis[27]. Clades I, III, and IV are more commonly associated with invasive disease and nosocomial outbreaks, while clades II and V have been primarily reported in cases of otomycosis and rarely in bloodstream infection[28]. Human mortality associated with *C. auris* candidaemia is potentially higher with clades I and IV than clade III, but this difference has not been shown to be statistically significant[29]. Clade and strain-specific genotypic and phenotypic variation in these traits have been described and may underlie differences in clinical presentation and pathogenesis.

Gene expression profiling *in vivo vs in vitro* conditions has become a standard approach for assessing host and pathogen responses to infection. To date, no experiment has described the gene expression of *C. auris* or its host during *in vivo* infection, although studies using human whole blood *ex vivo*[30], co-incubation with

human dermal fibroblasts[31] or murine cell line-derived macrophages[32] have provided useful insights. Additionally, host responses have been assessed in human peripheral blood-derived monocytes[33] and murine bone marrow-derived macrophages[34], but not in a living host. A dual RNA-seq study using the *ex vivo* whole blood model demonstrated similar host responses to several *Candida* species such as *C. albicans*, but identified a unique pattern of pathogen gene expression for *C. auris*, including up-regulation of transporter genes such as orthologues of the *C. albicans* siderophore transporter *SIT1*[30]. Interestingly, this family of predicted xenosiderophore transporter genes is significantly expanded in several members of the *Metschnikowiaceae* clade compared to other *Saccharomycetae*[23], raising questions as to the roles of siderophore transporters in *C. auris* biology[35].

The dearth of studies profiling host-pathogen gene expression *in vivo* for *C. auris* infection may be explained by multiple challenges. Most murine models, such as BALB/c[19,36–38] and C57BL/6 mice[34], have only very rarely demonstrated lethality through *C. auris* infection[33,39,40] without major immunosuppression with cyclophosphamide/cortisone[41–52], monoclonal antibody neutrophil depletion[20,53], or other immunodeficiency[21,54,55]. Additionally, mouse models are also expensive and associated with concerns over environmental pathogen shedding[56]. Alternative host models such as *Galleria mellonella*[36,46,57–63], *Drosophila melanogaster*[64] and *Caenorhabditis elegans*[62] have been employed, but these may lack key elements of mammalian-relevant immune systems, thus limiting their scope of application. In patients, immune control of *C. auris* is thought to depend on myeloid cell activity *via* C-type lectin receptors such as complement receptor 3 and mannose receptor MMR, followed by interleukin (IL)-17 pathway activation[65,66]. Therefore, an animal model that closely aligns with these mechanisms is required for human-relevant profiling of host-pathogen interactions.

Though the environmental origins of *C. auris* have not been conclusively demonstrated, a marine origin has been hypothesised and supported by successful

isolation of *C. auris* in coastal waters of both Indian and Pacific oceans[67,68]. Notably, a close relative of *C. auris* in the *Metschnikowiaceae* clade, *C. haemulonii*, was first isolated in 1961 from the gut of blue-striped grunt (genera name "*Haemulon*" for their blood-red mouth interior)[69]. Therefore, a marine halotolerant model could shed light on a possible evolutionarily adaptive niche. Fish larvae must survive hostile and varied ocean environments, demonstrating very early innate immune responses such as antimicrobial peptide production and the complement cascade[70,71]. Furthermore, adult teleost fish possess functional IL-17 subtypes (A and F) that lead to T-helper-17 subset differentiation and adaptive immunity in response to fungal infection[72]. The zebrafish (*Danio rerio*) model has allowed hindbrain[25,73] and swim bladder[74] microinjection modelling of *C. auris* infection, but rarely at temperatures above 30 °C, which zebrafish are broadly intolerant of. Again, we are unaware of any in-host transcription studies using the zebrafish model. Fungal transcriptional programmes can vary greatly across temperatures and are critical for mammalian pathogenesis[75–77]. A thermotolerant teleost fish embryo model such as the *Aphanius dispar*, also known as the Arabian killifish (AK), which can acclimatise to temperatures up to and including 40 °C[78–81] offers a balance between considerations of suitability for experimental manipulation, applicability to human fungal infection at mammalian temperatures, and relevance to hypothetical origins in an emerging pathogen.

In this paper, we present the first study exploring in-host virulence of *C. auris* clades I-V in the AK yolk-sac microinjection model at 37 °C, with sufficient power to detect significant differences in virulence. We supplemented our validation of the model with histology, fungal burden recovery, and dual host-pathogen RNA-seq. By comparing *in vivo* and *in vitro* expression profiles of *C. auris*, we detected a cross-clade expression signature that was significantly enriched for siderophore transporter *SIT1* paralogues, which mediate uptake of siderophores produced by other microbes (xenosiderophores). We designated this expanded gene family as xenosiderophore transporter candidates (*XTC*), which included a haem transport-related (*HTR*) sub-clade. We also identified *in vivo* filamentation by clade V during infection, which was associated with orthologues

of key hypha-associated genes from *C. albicans*. Together, these findings substantially enhance our knowledge of the processes underpinning *C. auris* infection.

Results

C. auris clades I-V are virulent in the AK microinjection model and clade V uniquely exhibits in-host filamentation

Microinjection of the AK yolk-sac with each of the five *C. auris* clades was lethal at 37 °C (91.7-100% 7-day mortality for each clade) compared to sham injection (5.6% mortality). Kaplan-Meier survival curves demonstrated a significantly higher lethality for clade I (*vs* II, III or V, $p < 0.001$) and clade IV (*vs* II or III, $p < 0.04$) (**Fig. 1A**; **Table S1**). Growth of the clade II strain in YPD-broth at 37 °C was noticeably slower over 24 h compared with other clades (**Fig. S1A**). However, colony-forming units (CFU) recovered post-infection from AK embryos were commensurate with similar in-host growth (**Fig. 1B**), with no differences identified between clades immediately post injection (x = 673 CFUs per infected embryo), 24 h post injection (HPI) (x = 1.12 x10^5) or 48 HPI (x = 1.78 x10^5), except between clade III and V at 48 HPI (x 4.48 x10^5 *vs* 1.56 x10^4, $p < 0.01$). These results indicate that AK embryo yolk-sac microinjection is a suitable model for the study of lethal *C. auris* infection at mammalian temperature.

Histological sectioning of the AK yolk-sac at 48 HPI revealed budding yeast morphologies, except for the clade V strain, which demonstrated predominantly filamentous forms (**Fig. 1C**). When grown in YPD-broth before microinjection, all isolates exhibited yeast morphologies; clade V colonies recovered from AK yolk-sac infection and grown on YPD-agar demonstrated rough (as opposed to smooth) colonies in approx. 1-2% of plated colonies (**Fig. S1B**), which consisted of elongated yeast cells and filamentous structures (> 10-50 µm) reminiscent of pseudohyphae (**Fig. S1C**). Death was defined by cessation of heartbeat, which was followed by yolk-sac collapse

visible by timelapse microscopy (**Fig. 1D**). These findings informed the study design for comparing *C. auris* gene expression between individual clades during *in vivo* and *in vitro* growth to detect drivers of phenotypic and morphological variation relevant to in-host virulence (**Fig. 1E**).

C. auris triggered host iron-nutritional immunity, heat shock response, and complement activation

To determine whether microinjection interefered with host transcriptional responses, we identified differentially expressed genes (DEGs) between sham injection and no injection, defined as genes with significant ± >2 log-fold change in expression after multiple testing. Though principle components analysis did not separate gene expression profiles (**Fig. S1D**), correlation clustering separated sham injection and negative controls without injection (**Fig. S1E**). However, there were only 30 DEGs for sham injection compared to no injection (0.11% detected genes; **Fig. 2A**), with up-regulation of zero and seven genes (at 24 and 48 HPI, respectively) and down-regulation of four and nineteen genes (24 and 48 HPI, respectively). Four GO terms were significantly enriched in the set of genes up-regulated at 48 HPI (relating to sarcomere generation, organisation, M-band and muscle) with no enriched KEGG pathways or PFAM domains, according to a falsed discovery rate (FDR) cut-off of 0.001. These GP terms were driven exclusively by three orthologues of murine *TITIN* (log-fold change x = 7.59, gene ratio 0.16), a ~ 3-4 MDa cardiac muscle protein with a putative role in haemodynamic stress tolerance and volume overload mechano-sensing (**Fig. 2B**). Other up-regulated genes included vascular adhesion molecules and hypothetical immunomodulator, dipeptidase 1 (*DPEP1*, **Table S2**). High survival of AK embryos receiving sham injection and minor changes in gene expression (consistent with physiological responses to exogenous fluid bolus) supported continued analysis of host responses to infection.

To characterise host responses to *C. auris* during infection, we identified host DEGs between infection by each clade and sham injection. Principle components analysis (**Fig. S1D**) and correlation clustering (**Fig S1F**) did not cluster gene expression profiles separately at either time-point (24 and 48 HPI). We identified 685 DEGs during infection with any clade (2.49% potential genes), of which 183 were up-regulated and 508 were down-regulated in response to at least one clade. There were no DEGs shared in common across host responses to all five clades, and only a small set of four up-regulated genes and one down-regulated gene shared across host responses to four clades of infection (**Table S2**). Up-regulated genes included Laminin subunit alpha-1 (*LAMA1*, not significant in response to clade III) and three genes that were not significant in response to clade II, Glucose-6-phosphatase (*G6PC*), DN117939 (hypothetical protein) and Tryptophan aminotransferase protein 1 (*TAR1*); immunoglobulin-like fibronectin type III domain-containing protein 1 (*IGFN1*) was down-regulated. These results suggest AK larvae have a subtle and non-uniform response to each clade of *C. auris* microinjection at these time-points, also reflecting levels of virulence and stages of infection.

We identified clade-specific AK responses to infection. At 24 HPI, clade II elicited the greatest host response, with up-regulation of 41 genes and down-regulation of 210 genes (**Fig. 2A**). However, at 48 HPI, clade IV elicited the greatest response (49 up-regulated, 104 down-regulated). Heat shock proteins (*HSP30* and *HSP70*, but not *HSP90*), complement cascade elements, pattern recognition receptors (PRRs), inflammatory transcription regulators, and modulators of nutritional immunity were differentially expressed with higher log-fold changes in clades I and IV, especially at 48 HPI (**Fig. 2C**). The most prominent gene relevant to pathogen recognition was *CARD14* in clade I and IV infection at 48 HPI (**Fig. 2D and 2E**). We found *NLRP3* (inflammasome) expression during clade III infection at 24 HPI only. There was no significant differential expression of several fungal immune response orthologues, such as *IL-17*, for infection with any clade. Together, these findings suggest that heat shock proteins, nutritional immunity, and the complement effector system are important

elements of the AK larval response to *C. auris* microinjection at 37 °C.

In order to highlight the roles of gene families in the host repsonse, we annotated the AK transcriptome and identified enriched GO terms, KEGG pathways and PFAM domains. Most significantly enriched gene features were identified from responses to infection with the more virulent clades (I and IV) at 48 HPI (**Fig. S2**). The highest mean log-fold changes for any enriched gene features were for clade IV infection, with haem catabolism, haem binding, and haem oxygenase (*HMOX*) related GO terms, KEGG pathway and PFAM domains. Two host orthologues of *HMOX* drove most of these enrichments, such as haem oxidation (log-fold change x = 3.96, FDR < 0.0003, **Fig. 2E**). In terms of other genes involved in iron-nutritional immunity, the AK also up-regulated Ferroxidase Hephaestin (*HPHL1*) in response to clade IV infection, but not Hepcidin (*HEPC1*). The response to clade I infection included 15 enriched GO terms, driven by up-regulation of two orthologues of Laminin subunit-α (*LAMA1*, *LAMA2*, **Fig. 2D**). No GO terms, KEGG pathways, or PFAM domains were enriched across responses to all five clades. Only one GO term was enriched across responses to four clades, which related to sarcomeric Z-disc in down-regulated genes at 48 HPI (II-V), driven by genes involved in connective and muscular tissue, including *IGFN1* and Calpain-3 (*CAN3*). The response to clade IV infection, in particular, indicates activation of iron metabolism and sequestration, potentially comprising an iron-nutritional immunity response to infection.

C. auris xenosiderophore transporter expression was enriched across all five clades during in-host infection

To identify infection-specific *C. auris* gene expression, we compared the in-host transcriptome to expression induced by growth in a standard rich laboratory media (YPD). Principle components and sample correlation clustering from gene expression data indicated a predominant separate clustering of *in vivo vs in vitro* conditions, indicating that the gene expression profile of *C. auris* during infection is substantially

267 different to that when it is grown in nutrient-rich laboratory media (**Fig. S1G and S1H**).
268 We identified 960 DEGs between *in vivo* AK infection at 24 HPI or 48 HPI *versus in vitro*
269 culture in YPD over 24 h (499 up-regulated, 523 down-regulated, 17.7% of potential
270 genes, **Fig. 3A**). We identified few DEGs between the two time-points 24 HPI to 48 HPI,
271 with zero DEGs for clade IV and V (**Fig. 3B**). Numbers of up-regulated DEGs unique to
272 any single set were highest for individual clades, particularly in the filamentous clade V
273 at 24 HPI and in the more virulent clades I and IV at 48 HPI (**Fig. 3C-D**). We annotated
274 clade-specific reference genomes, and performed differential expression to unveil
275 enriched gene features across all five clades. Six GO terms, KEGG terms or PFAM
276 domains were enriched across in-host all five clades at 48 HPI, related to major
277 facilitator superfamily carbohydrate and siderophore-iron transmembrane transport (**Fig.
278 S4**). This highlighted the expected importance of up-regulation of genes involved in
279 sugar uptake *in vivo vs in vitro*, but also raised the unexpected possibility that up-
280 regulation of members of the *C. auris* expanded gene family of siderophore transporters
281 could be a general feature of in-host infection.
282
283 To detect a signature of *in vivo* gene expression across the species, we identified
284 the set of 31 DEGs that were significant for all five clades of *C. auris* (**Fig. 3E, Table
285 S3**). Thirteen DEGs common to all clades of in-host transcripion were transmembrane
286 transporters, including up-regulation of transporters for xenosiderophores (*SIT1_3921*,
287 *SIT1_1487*), sugar (*HGT2*, *HGT12*), ammonia (*ATO2*), and nicotinic acid (*TNA1*), and
288 down-regulated drug-resistance-related efflux pumps (*MDR2* and *DTR1*) and peptide
289 transporters (*TPO3*, *PTR22*). Several putative virulence factors such as lipase *LIP1* and
290 cell wall-related *KRE6* and *SOD6* were also down-regulated across all five clades. We
291 demonstrated prominent DEGs (such as down-regulated *ALS4* and *MDR1*) that were
292 significant for at least one clade by mean log-fold change expression volcano plots (**Fig.
293 3F**). We also noted that several members of the *SIT1* family were differentially
294 expressed by at least one clade, but were not significant across all five clades, including
295 five genes that were significantly up-regulated across four clades (*SIT1_1542*,
296 *SIT1_1457*, *SIT1_1458*, *SIT1_2110*, and *SIT1_4097*) and five that were up-regulated in

one (*SIT1_0002* and *SIT1_2465*), two (*SIT1_3908* and *SIT1_2465*) or three clades (*SIT1_2241*). Two more family members were down-regulated across three clades (*SIT1_1519* and *SIT1_1499*). To nuance these findings further, we noted that two up-regulated genes were also down-regulated in one (*SIT1_3908*) or two clades (*SIT1_2465*). The many up-regulated members of the *SIT1* expanded gene family highlighted the potential importance of the wider family for in-host survival.

To examine orthologues across reference genomes for each clade (**Fig. S3**), we identified 5,324 orthogroups across clades I-V with outliers *C. haemulonii* and *C. albicans* containing 95.4% of all genes (*n* = 38,345 genes, **Fig. S3A-B**). The use of clade-specific reference genomes identified higher numbers of DEGs (692 *vs* 499 up-regulated and 714 *vs* 523 down-regulated genes) including genes within the accessory genome (55 *vs* 40 up-regulated and 57 *vs* 45 down-regulated, **Fig. S3C**), which we defined as orthogroups of genes not found in every clade. The core genome across all three species and five clades of *C. auris* included 3619 single copy orthologues (x = 66.9% *C. auris* genome per clade) and a further 869 single copy orthologues in *C. auris* (x = 82.9% *C. auris* genome per clade), of which 133 were unique to *C. auris*. The remaining core genome included 486-585 multiple copy orthologues shared across all species and 110-121 in *C. auris*, of which 17-19 were present in each clade (x = 643.2 genes per clade), bringing the total estimated core genome size to 5131.2/5413.2 genes per clade (x = 94.8%). A single copy orthologue tree confirmed the basal status of clade V, and synteny plotting was consistent with limited transversions/inversions within *C. auris* outwith clade II **Fig. S3A**. These findings are consistent with a highly conserved core yeast genome across *Candida* species, especially within the *Metschinikowiaceae* clade, which appears to contain a degree of preserved genome structure.

We observed high correlation between logFC values obtained from clade-specific and core (B8441) reference genomes (Pearson's >= 0.95, p <0.001 per comparison). Among DEGs that had no orthologues in the clade I reference genome (**Fig. S3D**), the

highest number of clade-unique genes that were differentially expressed was identified in clade IV; other DEGs included genes involved in cell wall, intracellular transport, metabolism, transcription/translation and transmembrane transport (**Table S3**). In terms of siderophore transporters, we additionally identified a clade IV unique gene associated with a siderophore transport GO term that was differentially expressed at both time-points of infection (CJJ09_005327). Overall, the *in vivo* expression profile across five *C. auris* clades indicated a potential role for the expanded gene family of siderophore transporters during *C. auris* in-host survival and pathogenicity, which was up-regulated compared to growth in nutrient-rich laboratory media.

More virulent *C. auris* clades I and IV up-regulated the non-mating *MTL* gene, *PIKA*, and down-regulated *MDR1*

Given significant differences in virulence between clades, we examined gene expression differences between clades I and IV (more virulent) and II and III (less virulent), excluding clade V due to its major morphological differences. We identified 623 up-regulated and 779 down-regulated DEGs expressed in clades I and IV, of which 14 were up-regulated and 22 were down-regulated across all comparisons. In order to explore potential drivers of virulence, we excluded DEGs that were significant only for *in vitro* comparisons and examined the remaining set of 10 DEGs shared across all *in vivo* comparisons (I *vs* II, I *vs* III, IV *vs* II, IV *vs* III, **Fig. 4A**, **Table S3**). Strikingly, three of these genes were non-mating genes located at the mating-type locus (*MTL*), including poly-A polymerase *PAP1*, oxysterol binding protein *OBPA* and phosphatidylinositol 4-kinase *PIKA* (**Fig. 4B**). Within the set of 10 DEGs shared across all comparisons, several genes outside the *MTL* were up-regulated, including vacuolar protein sorting gene, *VPS70*, and filamentous growth regulator, *FGR14*. Additionally, the drug efflux pump, *MDR1*, was down-regulated across all comparisons, supporting the idea of a fitness trade-off between resistance and virulence.

Notably, clades I and IV contain the **a**-type *MTL*, whereas clades II, IV and V contain the **α**-type *MTL*. That both *MTL* contain the non-mating genes is a conserved feature across *Candida* species, in which the *MTL**a*** and *MTL**α*** genes occupy alternative positions. Comparing transcript levels across *MTL* genes in all five clades, we observed poorer detection of *MTL**α*** transcripts when aligned to the clade I reference genome, as expected (**Fig. S5A**). Direct transcript-level testing, with correction for multiple testing to minimise false positives, indicated that only up-regulation of *PIKA* and *PGA30* (48 HPI) and down-regulation of *THI4* (24 HPI) and *MDR1* (at both time-points) were significantly different across the set of 10 DEGs shared across all comparisons (**Fig. S5B**).

We used the clade I reference genome to annotate functional domains and discover enriched gene families, revealing enrichment of up-regulated hypha-regulated cell wall GPI-anchored proteins in more virulent clades (**Fig. S4**), driven by three pairs of orthologues of *IFF4*, *HYR3* and *RBR3* (**Table S3**). Four secretory lipase *LIP1* paralogues drove an enrichment of the related PFAM domain for clade I *vs* III at 24 HPI. When comparing clade I and IV infection to clade II and 48 HPI, we also observed up-regulated nutrient transporters including a 7 transmembrane domain putative ferric reductase/iron importer, *CFL4*, as well as ferric reductase, *FRE3*, and siderophore transporter orthologues *SIT1_1948*, *SIT1_2241* and *SIT1_4097*. Cell wall components, non-mating *MTL* locus genes such as *PIKA*, and genes involved in iron and siderophore transport are therefore potential modulators of strain-specific differences in virulence.

Typical and atypical hypha formation programmes in basal clade V during AK yolk-sac infection

To explore drivers of filamentation by the clade V strain, we identified 1,046 DEGs between clade V and each of the other clades (I-IV), comprising 601 up-regulated and 526 down-regulated genes across all comparisons. We then identified a set of 57 genes shared across all comparisons for *in vivo* conditions only, since we did observe filamentation in nutrient-rich YPD. 22 genes were up-regulated at 24 HPI, 7 at 48 HPI,

and 18 at both time-points (**Fig. 4C**). The majority of up-regulated genes were metabolic (*n* = 13), including two cytochrome P450 *ERG5* orthologues, though *ERG11* was down-regulated. Transmembrane transporters for sugar (including two *HGT13* orthologues), amino acids and siderophores (*SIT1_1487*) were also up-regulated (*n* = 10). Cell wall genes up-regulated in filamentous clade V (*n* = 8) included the novel adhesin *SCF1*, GPI-anchored genes *PGA31* and *IFF4*, and orthologues of classical *C. albicans* hyphal adhesins *ALS3* and *RBR3*. We identified differentially expressed transcription factors and related regulators, such as *HAP41* and the pheromone receptor *STE2*, which could play a governing role on these responses. Given the minor differences in numbers of DEGs identified when using clade-specific reference genomes, we also compared the transcript levels for each gene in this set with annotations to identify a highly strict shortlist of inter-clade difference. Using this method, the only significant differences were for up-regulation of *MED7* and *SPS19* (at 24 HPI) and two *HGT13* orthologues and *RNH70* (at both time-points, **Fig. S6**).

We also examined significant DEGs between clade V and at least one other clade using mean-log fold change (**Fig. 4D**). Several genes that play critical roles in *C. albicans* hypha formation were highly up-regulated, such as transcription factor *UME6* and hypha-specific G1 cyclin-dependent protein serine/threonine kinase *HGC1*. Enrichment analysis indicated up-regulated gene sets involving CFEM domain, cytochrome P450/oxidoreductase activity, hypha-regulated cell wall GPI-anchored proteins and siderophore transport, particularly at 24 HPI and comparing clade V to clade II (**Fig. 4D**). Significantly up-regulated iron-related transport genes in clade V included *FRE3*, *CFL4*, *FRP1*, *SIT1_1519*, *SIT1_1487*, *SIT1_4097*, *SIT1_1542*, and *SIT1_1499*. These findings are consistent with the preservation of a major filamentation programme in *C. auris*, demonstrated in the basal clade V, with unique characteristics such as expression of *SCF1* and the up-regulation of several members of the expanded family of siderophore transmembrane transporters.

Xenosiderophore transporters are a *Metschnikowiaceae*-specific expanded gene family with varied expression patterns in *C. auris* infection

Given the prominence of *SIT1* orthologues across the transcriptomic analyses of *C. auris* during *in vivo* gene expression, we set out to characterise the expanded gene family across orthogroups, including outgroup species *C. haemulonii* and *C. albicans*. **Fig. 5A** shows the predicted structure of *Sit1_1542* (AlphaFold 3). Blastp searches identified proteins with sequence similarity across seven orthologue clusters, of which two main groupings of transporters with 14 transmembrane domains (TMRs) emerged (**Fig. 5B**). A larger branch was annotated with GO term, KEGG pathway and PFAM domains relating to siderophore import (including 12 genes in clade I), and a smaller branch was annotated with GO terms relating to haem transmembrane import (including 5 genes in clade I). The majority of orthologues retained 14 TMRs, and few had evidence of additional annotations except for the trichothecene mycotoxin efflux pump PFAM domain across multiple groupings. The orthologue *SIT1_1547* contained 12 TMRs and was up-regulated with *SIT1_1548* containing 2 TMRs, which was not identified as a *SIT1* orthologue in our pipeline but has previously been described as such[30,82].

Co-expression analysis, using an unweighted network (Pearson's correlation) with a cut-off of 0.85, demonstrated eight clusters featuring *SIT1* orthologues, one of which included five that were co-expressed (**Fig. 5C**). To understand how our *in vivo* expression of *C. auris* compared to other experimental conditions previously reported, we measured gene expression across publicly available RNA-seq datasets, identifying 35 datasets for which we were able to ascertain gene expression using our pipeline, but none of which included an in-host setting (**Table S4**). Gene expression patterns within the set of single copy orthologues clustered within both principal components analysis of experimental unit variance (**Fig. S3E**) and hierarchical clustering of $\log_{10}$ variance per gene (**Fig. 3F**). We used this data to construct an additional unweighted co-expression network as above for *SIT1* orthologues among single copy orthologue genes, identifying

two clusters only, featuring *SIT1_2110* and *SIT1_1519* (**Fig. 5D**). Given the difference in co-expression patterns between the responses identified in the AK marine host across this study, and a broader meta-analysis of available RNA-seq data, these results highlight a potentially unique influence of a marine larval host environment on transcription programmes and the need to explore in-host time series data with weighted co-expression networks in the future.

To explore the evolutionary history of *SIT1*-related genes in fungi, we performed Blastp searches for orthologues of *C. albicans SIT1* using an e-value cut-off of $1e^{-20}$ across 226 fungal species' reference genomes totalling 304 genomes. Separately, 28 *Oomycota* genomes were found to contain zero orthologues. We identified 1,689 hits, which clustered into two branches: a smaller branch (*n* = 397) annotated for siderophore transport including the 12 *C. auris* groupings which we have designated "xenosiderophore transporter candidates" (*XTC*), and a larger branch (*n* = 1,292) featuring genes predicted (by GO term) to encode haem transporters, including the 5 *C. auris* groupings, which we have additionally designated "haem transport-related" (*HTR*, **Fig. 6A**). There were no putative haem transporters or members of the larger branch for *C. albicans*, which only contained the single *SIT1* gene. We calculated the mean number of orthogroups per genome per species (**Fig. 6B**). This showed the most prominent expansion of the *XTC* branch in the *Metschnikowiaceae* clade, including *C. auris* (12 orthologues) and even more so in *C. haemulonii*, with 15 orthologues. No other fungal species or group of species contained so many. *XTC* orthologues were not present in any members of the basal blasocladiomycota, chytridiomycota and mucoromycota, or in several ascomycota (e.g. *Pichia kudriavzevii*, *Schizosaccharomyces pombe* and *Pyricularia oryzae*) and basidiomycota (e.g. *Ustilago maydis*). Common human fungal pathogens such as *Aspergillus fumigatus*, *C. albicans* and *Nakaseomyces glabratus* contained only one *XTC* orthologue (**Fig. 6B**). The *HTR* clade, by contrast, was more prominent across fungal phyla, with as many as nine in *Mucor* species, 16 in *A. flavus* and 22 in *F. solani*. We therefore propose a naming of these two expanded gene families as *XTC1-12* and *HTR1-5* in *C. auris*.

We note the absence of *XTC5* in clade V, *XTC10* in clade IV, and in addition to these, *XTC4*, *XTC9* and *XTC11* in clade II (**Fig. 6C**). Interestingly, clade II, which exhibits the greatest degree of *XTC* gene loss, is also considered to be the least virulent strain. It is also noteworthy that the AK embryo expressed *HMOX* genes during clade IV infection, while clade IV *C. auris* up-regulated *HTR1*, *HTR2* and *HTR5*. This suggests a specific host-pathogen interaction axis in nutritional immunity related to haem scavenging. No other clades of infection were associated with such iron-related functional enrichment in the host, and no other clades expressed more than one *HTR* gene (except *HTR1* and *HTR5* in clade III at 48 HPI). Clade II down-regulated *HTR1* in-host. In summary, *XTC1*, *XTC2*, *XTC3*, *XTC4*, *XTC6*, *XTC7*, *XTC11* and *XTC12* were up-regulated while *XTC8*, *XTC9* and *XTC12* were down-regulated *in vivo* in at least one clade, while up-regulation of *XTC3* and *XTC7* was significant across all clades. Additionally, the more virulent clades were associated with up-regulation of *XTC4, XTC5,* and *XTC11*. The filamentous clade V up-regulated *XTC7* across comparisons with all other clades, and up-regulated *XTC1, XTC4, XTC8* and *XTC9* compared to at least one other clade.

Discussion

We have desribed a model for comparative functional genomics of *C. auris* in-host survival using AK yolk-sac microinjections at a clinically relevant temperature. All five clades demonstrated similar lethality, with a minor but significant increase in pathogenicity for clades I and IV, consistent with clinical and laboratory findings[29]. In-host growth was similar across all clades and high enough to indicate a large enough *in vivo* fungal burden for robust bulk transcription assessment across the species. Lower CFUs in clade V could be explained by increased aggregation of filamentous cells. The contained nature of the yolk-sac provides a straightforward experimental unit of host tissue without the challenges of pathogen RNA isolation such as locating foci of infection in larger animals. Additional time-points at could be an informative future area

of study to develop fine-resolution strain-specific transcription networks. Thus, an AK yolk-sac microinjection model has the potential to fill a substantial need for *in vivo* gene expression studies in general.

We investigated the host transcriptional response to *C. auris* infection. The most highly up-regulated gene family included two heme oxygenase (*HMOX*) genes. *HMOX* genes have been shown to mask iron from invading pathogens as a feature of anti-*Candida* nutritional immunity[83], so presumably have a similar function against *C. auris*. This was particularly notable given *HMOX* genes were up-regulated in response to clade IV infection, and the clade IV isolate had a corresponding significant up-regulation of 3 haem transport-related *HTR* genes. In addition to nutritional immunity genes, we found up-regulated heat shock and complement cascade genes during infection, confirming the expected immune response to fungal infection[65,66]. Genes with complex roles in immunity were up-regulated, such as *NLRP3*, for which *C. auris* may be less activating than e.g. *C. albicans*[27,84]. It is notable that the yolk-sac model was not associated with histological or transcriptional evidence of host neutrophil recruitment and activation, a prominent feature of human blood infection modelling[30]. Reference genome bias resulting from the available adult gill transcriptome assembly[85] may limit detection of host gene expression features, so future long and short read assembly from gene expression data across a range of larval stages could further understanding of AK immunity.

We discovered a complex pattern of differential expression by *C. auris* during infection compared with *in vitro* conditions. The lack of a major distinction across time-points (24 *vs* 48 HPI) indicates that the transcriptional activity of *C. auris* in-host was highly similar at these stages. Six functional annotation terms (GO, KEGG pathway and PFAM domain) were significantly enriched among genes that were up-regulated across all five clades, including sugar and siderophore transporters. The enrichment of sugar transporters outside of nutrient-rich YPD-broth is unsurprising, such as High-affinity Glucose Transporter *HGT12*, with evidence of redundancy in *C. albicans*[86–89], and

534 *HGT2*, part of an eight-gene "core filamentation response network" in *C. albicans*[90].
535 More surprising was the down-regulation of putative virulence factors such as Secreted
536 Aspartyl Protease 3 (*SAP3*), thought to be the most important SAP in *C. auris*, and
537 required for virulence in a mouse model[26], and Copper Superoxide Dismutase *SOD6*,
538 which has been shown to be down-regulated in iron starvation[91]. Multi-drug efflux
539 pumps such as *MDR2* (down-regulated *in vivo*) and *MDR1* (down-regulated *in vivo* and
540 in clades I and IV *vs* clades II and III) are understood to drive drug resistance through
541 multiple but unclear mechanisms in *C. auris*[92,93]; in-host down-regulation may indicate a
542 fitness trade-off for virulence *vs* drug resistance.
543
544 The mating type locus (*MTL*) genes have been hypothesised to contribute to
545 virulence in fungal species including *Cryptococcus neoformans*[94]. Given that *C. auris* is
546 assumed not to undergo meiotic recombination[95], there is a question of what role *MTL*-
547 associated genes play in pathogenicity and morphology. Two of the three non-mating
548 genes (*PAP1* and *PIKA*) in the *MTL* were up-regulated by more virulent strains (I and
549 IV) compared to the less virulent strains (II and III). Importantly, the two more virulent
550 clades (I and IV) contain *MTL**a*** rather than *MTL**α*** (clades II & III)[23], and clades V and VI
551 contain *MTL**a*** and *MTL**α*** respectively[12]. Thus, it is unclear if the up-regulation of non-
552 mating genes is a *MTL* specific transcriptional nuance, or a feature of more highly
553 virulent *C. auris* clades. The *MTL* also did not feature prominently in the filamentation
554 response observed in clade V, providing no evidence for an obvious role for the *MTL* in
555 such morphological changes.
556
557 Filamentation is an important pathogenicity trait in fungi, especially *Candida*
558 species, although its roles have been more poorly described in aquatic infections[96]. We
559 observed *in vivo* filamentation by a representative strain of *C. auris* clade V, the
560 basal/ancestral clade[97], accompanied by a genera-typical filamentous gene expression
561 signature. Specifically, we measured the up-regulation of *HGC1* and *UME6*, which are
562 two of the most important regulators of filamentation in *C. albicans*, and have recently
563 been described as drivers of *C. auris* filamentation and biofilm formation[98]. The

expression of adhesin *SCF1* in filamenting clade V is noteworthy because its cationic adhesion mechanism has been postulated to be consistent with adhesion mechanisms common to marine organisms including bivalves[21]. The generalist marine-isolated pathogen *C. haemulonii* has also displayed filamentation competence at lower temperatures[99], consistent with an ancestral aquatic state.

Human histopathology reports of *C. auris* infection are rarely published and have not demonstrated classical in-host filamentation, to our knowledge. An *ex vivo* human epithelial model using a clade I isolate did demonstrate filamentous *C. auris* at 37 °C after injection into deeper dermis[100]. Clade III *C. auris* has also been observed to form filamentous/hyphal forms in *Galleria mellonella* injection[60]. Fan and colleagues have observed filamentous forms of *C. auris* across all four clades, even demonstrating a higher virulence in the *G. mellonella* model[101], though the phenotype required passage through a murine host with additional prolonged growth at 25 °C for at least 5 days before and after injection[19]. Other stimuli have induced filamentation in clade I isolates, such as hydroxyurea genotoxic stress[102] and Hsp90 inhibition[103], where several up-regulated genes in *C. auris* filamentation (*SCF1*, *IFF4* and *PGA31*) matched those in our study. Constitutive filamentous growth has also been demonstrated with a transposon-mediated disruption of a long non-coding RNA[104], which sit adjacent to chitin deacetylase *CDA2*, which was down-regulated at 24 HPI in this experiment during filamentation. These findings indicate that hyphal formation is possible across *C. auris* clades.

A total of twelve siderophore transporters were up-regulated during infection, and four were down-regulated, with three family members up-regulated in more virulent clades and five in the filamentous clade V. Siderophore synthesis may be unlikely in *C. auris*, given the lack of evidence in other *Candida* species[105]. As a result, *C. albicans* Sit1 - which is required for required for virulence[106] - is thought to be a xenosiderophore transporter for iron-chelators produced by other microbes and specific to the ferrioxamine type common in iron-poor ocean environments[107,108]. Siderophore

transporters can also act intracellularly for compartments such as the mitochondrion[109,110], or act as efflux pumps for various molecules[111] including trichothecene mycotoxins as identified by our functional annotations.

C. auris encodes a large expanded gene family of 17 siderophore transporters that we named xenosiderophore transporter candidates (*XTC*) 1-12 and haem transport-related (*HTR*) genes 1-5, the latter sharing sequence similarity with *S. pombe* low-affinity haem transporter Str3[112]. In other *Candida* species such as *C. albicans*, iron assimilation is understood to be central for in-host survival[113,114], where deprivation triggers various pathogenic programmes such as alterations in cell surface beta-glucan[115]. Haem is acquired by *C. albicans* through vesicular endocytosis and CFEM-domain containing proteins[116,117] and does not contain *HTR* genes, suggesting a possible loss of transmembrane haem transporters. The ubiquity of *HTR* across the fungal kingdom and lack of *XTC* genes in the three basal fungal phyla suggest that *SIT1*/*HTC* could have arisen from a duplication of an *HTR*-related gene in the Dikarya (the ascomycota and basidiomycota) with subsequent independent loss of both *XTC* and *HTC* genes in multiple fungal lineages. Our identification of up-regulated *XTC* transport during infection corroborates the findings of up-regulated *XTC2A-B* (*B9J08_1547-8*) in an *ex vivo* blood model of *C. auris* infection[30]. These findings together suggest the importance of iron during infection, which could be targeted in the clinic, e.g. via low-toxicity pyrvinium pamoate[118].

We show for the first time an *in vivo* transcriptional profile for the global public health threat and critical priority WHO human fungal pathogen *C. auris*. Representative strains from all five major clades of the recent simultaneous emergences highlighted strain-specific differences in morphology, virulence and gene expression. This study highlights the advantages and potential of a thermotolerant yolk-sac injection model, adding to the debate around the putative marine origins of *C. auris*, and the emergence of distinct clades. We demonstrate natural filamentation by clade V and virulence advantages of clades I and IV, and comprehensively describe the associated gene

expression. We indicate the importance of the *XTC* and *HTR* gene clusters as recommended targets for investigation of fungal biology, pathogenicity and treatment. Our findings shed new light on the emergence and evolution of *C. auris* from a marine yeast ancestor. Our analyses reveal new potential drug targets that enable *C. auris* to survive in aquatic hosts, which may have a similar function during human infection, with implications for patient care and public health control.

Methods

Ethical Statement: All animal experiments were performed under Project Licence PP4402521 in compliance with University of Exeter Animal Welfare Ethical Review Board regulations and MRC Center for Medical Mycology Project Review Board, and are reported in line with "Animal Research: Reporting *in vivo* Experiments" (ARRIVE 2.0) Guidelines[119].

***Aphanius dispar* Care, Monitoring, Husbandry and Procedures:** Wild-type adult AK were kept at the Aquatic Resources Facility, Exeter, in two 28 °C incubation tanks, with 12-hour day and night light cycles and artificial enrichment foliage. Embryos were collected using three plastic netted collection chambers per tank with transfer of all enrichment into tanks, and placed overnight from 16:00 to 09:15 in dark conditions. Chambers were then drained, cleaned and strained with 35 parts per thousand artificial seawater (ASW) to isolate all embryos. Subsequent ASW was sterile suction filtered *via* 0.2 µm pore Nalgene Rapid-Flow (Thermo Scientific, UK). Embryos were inspected for viability in terms of an intact blastocyst without discolouration by stereo dissection microscope (Optech, UK) and incubated at 30 °C (Memmert, Germany) for 72 h with day and night cycles with daily ASW changes and removal of dead, unhealthy or underdeveloped embryos, with a maximum of 30 embryos per standard size 100 mm x 15 mm petri dish (Greiner Bio-One, Austria). Excluded embryos were killed or disposed

of either by submission in Virkon solution (Sigma-Aldrich, UK) or freezing at -80 °C.

Experimental Procedures: Injection needles were prepared using borosilicate glass capillaries (Harvard apparatus, USA) and a heated pulling system (heater level > 62, PC-10, Narishige, UK). We used tweezers to snap the tip to an estimated 1 mm graticule-measured aperture of 10-20 µm, and sterilised needles before use with 253.7 nm UV light over 15 minutes (Environmental Validation Solutions, UK). Injection bays were made with microwaved 1% agarose in 1 g (Sigma, USA) per 100 mL ASW for up to 24 embryos in 100 mm petri dishes using custom-made molds in an inverted 60 mm petri dish. Embryos were randomly chosen from each dish and the sequence of injection for each biological repeat was randomly allocated by computer. For microinjection, *C. auris* yeasts were counted by haemocytometer and added to 25 µL sterile filtered phenol red solution 0.5% (Sigma, UK) to a concentration of 0.5×10^8 per mL in 100 µL. Injection needles were loaded with 5 µL injection solution using 20 µL Microloader EpT.I.P.S. (Eppendorf, UK) immediately before injection of up to 30 embryos before re-loading. Injections were performed with 400-500 hPa injection pressure and 7-40 hPa compensation pressure over 100-200 ms with the FemtoJet 4i (Eppendorf UK) using a micromanipulator (World Precision Instruments, UK) and a Microtec HM-3 stereo dissection microscope (Optech, UK). In order to deliver a dose of approx. 500 yeasts in 10 nL solution, an injection bolus was administered to an estimated diameter of 0.2 – 0.3 mm (10-15% of total embryo diameter) *via* a single chorion puncture. Any embryos that failed to meet these criteria for injection were excluded. Control *in vitro* inoculations were microinjected as above into 1 mL YPD in 1.5 mL Eppendorf tubes before incubation without shaking at 37 °C for 24 h contemporaneously with embryos as below.

Study Design and Sample Sizes: We used an unblinded prospective virulence study comparing six groups of AK embryo yolk-sac microinjection, including five different clades of *C. auris*, and one control sham injection as the negative control. We used >= 23 embryos per condition based on our power calculation of $\sigma = 0.25$,

significance = 0.05, power = 0.9, and δ effect size of 25% mortality (two-sided t-test). After excluding embryos that were unhealthy or did not complete successful microinjection, we included *n* = 10-13 embryos per group per experiment (total *n* = 34-37 embryos per group). Each embryo was considered to be an experimental unit (*n* = 70-72 embryos per experiment, total *n* = 213 embryos). For estimation of *C. auris* in-host growth by homogenisation and plating of colony forming units, three embryos per condition per time-point across two (0 and 24 HPI) or three (48 HPI) experiments were used (total *n* = 126). For time lapse microscopy demonstration of *A. dispar* yolk-sac collapse and death, representative image sets were chosen from a pilot experiment using a reduced dosage (1/10) of *C. auris* (*n* = 4). For histological demonstration of *C. auris* morphology, one embryo per condition at 24 HPI and 48 HPI each were used in one experiment, and seven embryos per condition plus three embryos without injection in a second experiment (*n* = 57). RNA was extracted from three embryos per condition per time-point (0, 24 and 48 HPI, *n* = 54) plus three embryos per time-point without any injection (*n* = 9, total *n* = 63) as a control for the impact of microinjection.

***C. auris* Strains and Growth:** We selected five *C. auris* strains to represent each major clade (**Table S1**). Culture stocks were kept in -80 °C in Yeast extract Peptone Dextrose (YPD) broth (Sigma-Aldrich, UK) containing 25% glycerol (ThermoFisher, UK) and plated onto YPD-agar (Sigma-Aldrich) for 48 h before innoculation and overnight growth in 10 mL YPD broth at 30 °C in a shaking incubator at 200 rpm (Multitron, Infors HT, UK). Five mL from each overnight culture was then centrifuged at 5000 g for 2 minutes before re-suspending and triple washing in 1 mL autoclaved deionised water (DIW, Milli-Q, Merck, USA) to prevent aggregation[22] then re-suspended in 200 µL DIW. Decontamination of surfaces was conducted with both mopping and cleaning wipes in 70% Ethanol (Sigma-Aldrich) or 10% Chemgene HLD_4L (Medimark Scientific, UK) as per manufacturer's instructions. For growth curves, *C. auris* strains were grown overnight in YPD in 4 replicates. Overnight cultures were inoculated into YPD to a final OD 600 of 0.02 in a 96-well plate. OD was read over 25 hourly cycles at 37 °C with 300 s shaking at 2.5 mm amplitude on an Infinite 200 PRO

plate reader (Tecan, Switzerland).

Outcome measurement: individual embryos were kept in 1 mL sterile filtered ASW per embryo in a 48 well flat bottom plate (Corning, USA) sealed with Parafilm “M” (Bemis Company, USA) at 37 °C with passive humidification using a 500 mL open glass beaker of water. Embryos were monitored for presence of heart rate at 24-hourly intervals up to 7 days by stereo dissection microscope. Initial time of injection was subtracted from each time-point to minimise bias between groups. Kaplan-Meier survival curves were plotted with Log-Rank testing and Benjamini-Hochberg (BH) correction[120] using survival v.3.5.8 and survminer v.0.4.9 packages in R v.4.4.0. Colony forming units (CFUs) were calculated by homogenisation of embryos at 0, 24, and 48 HPI by autoclaved plastic micropestle in a 1.5 mL conical tube (Eppendorf, UK) in 100 µL 10,000 U/mL penicillin/streptomycin (P/S) solution (Gibco, UK). Dilutions were made with P/S solution and DIW in 1/10-10,000 and counts were adjusted according to dilution after plating onto YPD agar plates and read after 72 h incubation at 30 °C. Statistical testing between CFU numbers was performed with Wilcoxon testing and BH correction.

Imaging: For direct microscopy, AK were kept in 300 µL ASW containing 0.04% Tricaine anaesthesia (Sigma-Aldrich, UK) in an optical adhesive and parafilm-sealed 96-well plate. These were then monitored for heart beat by 5 bright field 2X or 4X images at pre-focused z slices taken every 2 h by Acquifer microscopy (Bruker, Germany) over 72 h. All images were processed in ImageJ 1.53a (NIH, USA). Sectioning and staining was performed by Microtechnical Services, Exeter, UK, with fixation of embryos in 1 mL 10% neutral-buffered formalin (Sigma-Aldrich, UK) for > 24 h, followed by immersion in 4% phenol 10 mL glycerine BP made up to 100 mL with distilled water[121], sectioned at 4 µm without orientation, and stained with Harris Haematoxylin & 1% Alcoholic Eosin on Leica Autostainer. H&E stained histological sections were imaged on an Olympus IX83 microscope coupled with an Olympus DP23 colour camera using an Olympus UPlanXApo x40/0.95 objective controlled by cellSens

software v.3.2. Brightfield microscopy was performed with an EVOS M5000 microscope (ThermoFisher, UK). Microscopy of YPD-agar grown colonies was performed without staining in DIW.

RNA Extraction and Sequencing: Total RNA was extracted using the Monarch® Total RNA Miniprep Kit (NEB, USA). Embryos were flash frozen in liquid nitrogen, re-suspended in DNA/RNA Protection Reagent and disrupted with an autoclaved plastic micropestle. Bead beating was performed in a FastPrep 24 homogeniser (MP Biomedicals) with 0.5 mm zirconia/silica beads for 8 cycles of 35 s at 6 m/s plus 45 s on ice. Lysate was recovered and incubated for 5 min. at 55 °C with proteinase K before addition of lysis buffer and RNA purification following manufacturer's instructions. Total RNA samples were quantified using the Qubit 4.0 Fluorometer (Invitrogen, USA) and integrity was checked with the Tapestation 4200 (Agilent, USA). Library preparation and sequencing were performed by the Exeter Sequencing Service. Samples were normalised and prepared using the NEBNext Ultra II Directional RNA Library Prep - Poly(A) mRNA Magnetic Isolation Module following the standard protocol. Libraries were sequenced on a Novaseq 6000 sequencer with 150bp paired-end reads. Reads were trimmed with fastp[122] v.0.23.1 to remove reads < 75 bases and trim based from the 3' end with q-score < 22. Quality control was performed with FastQC (https://github.com/s-andrews/FastQC) v.0.11.9 and MultiQC[123] v.1.6.

Differential Gene Expression: We aligned sequences (x = 52.9 m reads per replicate, range 41.1-112.2 m) using the Trinity pipeline[124] v.2.15.1 to the *C. auris* clade I B8441 reference genome (GCA_002759435.2)[23] downloaded from GenBank (mean aligned reads in infected embryos 3.83 m, 0.81-13.1%). We further aligned clade-specific reference genomes for each strain (**Table S1**), including clade II (GCA_003013715.2)[4], III (GCA_002775015.1)[13], IV (GCA_008275145.1)[13] and V (GCA_016809505.1)[97,125,126]. We aligned conditions containing *A. dispar* to the *de novo* GJEY01 adult gill transcriptome assembly[85] downloaded from GenBank, for which we detected expression over 27,481 potential genes. Alignment was performed with

Bowtie2[127] v.2.5.1, transcript estimation with RNA Seq by Expectation Maximisation (RSEM)[128] v.1.3.3, differential expression with EdgeR[129] v.3.40.0, Samtools[130] v.1.17 and limma[131] v.3.54.0 using a false discovery rate (FDR) p-value cut-off of 0.001 and a log fold change cut-off of +/-2.0. Principal components were calculated and plotted using the prcomp function in Rv4.4.0 and ggfortify v.0.4.17 R package for fragments per kilobase per million, and correlations plots from counts per million as per the default output of the Trinity pipeline. Log fold change was plotted with ComplexHeatmap[132].

Annotation and Enrichment: Gene ontology terms[133,134] were assigned using DIAMOND[135] v.2.1.8 *via* the DIAMOND2GO pipeline[136] for each of the *C. auris* reference genomes. KEGG terms[137] were assigned using the BlastKOALA online platform using the eukaryote database[138]. Protein FAMily (PFAM) domains[139] were identified using the PFAM-A.hmm database (https://ftp.ebi.ac.uk/pub/databases/Pfam/current_release/Pfam-A.full.gz) and HMMER and HMM Scan[140] with a cut-off of $1e^{-5}$. Further domain-specific identification was performed with SignalP 5.0[141], DeepTMHMM 1.0[142] and NetGPI 1.1[143]. Enrichment analysis for DEG subsets was calculated using the Fisher's Exact test, adjusted using the Benjamini-Hochberg method per set of up-regulated or down-regulated features in each comparison as a conservative estimate of significant gene set enrichment, with a false discovery rate cutoff of p=0.001. Annotation tables were checked with additional information from available literature, supplemented by details and web-scraped orthologue names from *Candida* Genome Database[82] and Blastp searches[144]. Annotations for the GJEY01 genome were also performed using Diamond2GO, BlastKoala and HMMScan as above and checked against *A. dispar* annotations and gene names obtained directly from the GJEY01 transcriptome makers[85]. For plotting, lists of GO terms were identified (and for *A. dispar* enrichment, reduced by removal of redundant terms) by REVIGO[145].

Orthologue Assignment: To identify accessory genes across *C. auris* clades, we used the Synima pipeline[146] with Orthofinder v2.5.5[147] with additional reference

genomes for *C. albicans* (SC5314_GCA_000182965.3) and *C. haemulonii* (B11899_ASM1933202v1). We also incorporated a very recent version of the *C. auris* B8441 assembly (v3) to arrange contigs and illustrate re-arrangements, with broad syntenic concordance; it contains 5 more genes than v2, for which 27 (0.5%) and 16 (0.3%) genes were unique to each genome, respectively. Multiple alignment of single copy orthologues as defined by Orthofinder was performed with Muscle v5.1[148] and a phylogeny was made with FastTree v2.1.11[149] using default settings.

RNA-Seq Meta-Analysis Variance: NCBI SRA was searched for "*Candida auris*" on 16th April 2024 and downloaded as metadata *via* the "Send to: Run Selector" function. Each project accession number for runs containing RNA was searched against available published literature to identify publications, noting subject of study, clades/strains, growth media, comparative conditions, temperature and time scales used. Calculation of FPKM was performed and analysed as above using the set of single copy orthologues to demonstrate variance via PCA with ggfortify and prcomp packages in R and to calculate an unweighted co-expression network for *SIT1* genes with and without the additional data from the RNA-Seq meta-analysis, using Pearson's correlation with a correlation cut-off of 0.85.

***SIT1* Analysis:** The protein transcript for *C. albicans SIT1* was Blastp searched against the draft pangenome database as above. We visualised the structure using Alphafold v3[150] and ChimeraX v1.8[151]. Clade I-V *C. auris* and *C. haemulonii SIT1* genes were aligned using Muscle as above before using RAXML-NG v1.2.2 with 1000 bootstraps and the LG4X model[152], which was visualised using ggtree v3.12.0 and gheatmap. For panfungal *SIT1* analysis, we used the fungidb portal for Blastp using the *C. albicans SIT1* against all available fungal data (with no hits within oomyceta), including 274 reference genomes representing 197 species and a cut-off of $1e^{-20}$. Annotations for each protein transcript were performed as above to obtain GO terms, KEGG pathways, PFAM domains, GPI-anchors, SignalP domains, and transmembrane domains, while a phylogeny for *SIT1* similar sequences across all fungal references was

constructed as above following multiple alignment with Clustal Omega v1.2.4[153]

Data Availability: Raw reads have been deposited via NCBI/GEO *via* accession GSE277854. All datasets and code required to make figures are available via Github (https://github.com/hughgifford/Arabian_Killifish_C_auris_2024).

References

1. Meis, J. F. & Chowdhary, A. *Candida auris*: A global fungal public health threat. *The Lancet Infectious Diseases* **18**, 1298–1299 (2018).

2. WHO. World Health Organisation (WHO) fungal priority pathogens list to guide research, development and public health action. (2022) doi:https://www.who.int/publications/i/item/9789240060241.

3. Lee, W. G. *et al.* First three reported cases of nosocomial fungemia caused by *Candida auris*. *Journal of Clinical Microbiology* **49**, 4 (2011).

4. Satoh, K. *et al.* *Candida auris* sp. Nov., a novel ascomycetous yeast isolated from the external ear canal of an inpatient in a Japanese hospital. *Microbiology and Immunology* **53**, 41–44 (2009).

5. Lyman, M. Notes from the field: Transmission of pan-resistant and echinocandin-resistant *Candida auris* in health care facilities - Texas and the District of Columbia, January-April 2021. *Morbidity and Mortality Weekly Report* **70**, (2021).

6. Eyre, D. W. *et al.* A *Candida auris* outbreak and its control in an intensive care setting. *New England Journal of Medicine* **379**, 1322–1331 (2018).

7. Taori, S. K. *et al.* *Candida auris* outbreak: Mortality, interventions and cost of sustaining control. *Journal of Infection* **79**, 601–611 (2019).

8. Shuping, L. *et al.* High prevalence of *Candida auris* colonization during protracted neonatal unit outbreak, South Africa. *Emerging Infectious Diseases* (2023) doi:10.3201/eid2909.230393.

9. Adam, R. D. *et al.* Analysis of *Candida auris* fungemia at a single facility in Kenya. *International Journal of Infectious Diseases* **85**, 182–187 (2019).

10. Prayag, P. S., Patwardhan, S., Panchakshari, S., Rajhans, P. A. & Prayag, A. The dominance of *Candida auris*: A single-center experience of 79 episodes of candidemia from Western India. *Indian Journal of Critical Care Medicine* **26**, 560–563 (2022).

11. Khan, T. *et al.* Emergence of the novel sixth *Candida auris* Clade VI in Bangladesh. *Microbiology Spectrum* **12**, e03540–23 (2024).

12. Suphavilai, C. *et al.* Detection and characterisation of a sixth *Candida auris* clade in Singapore: A genomic and phenotypic study. *Lancet Microbe* **0**, (2024).

13. Lockhart, S. R. *et al.* Simultaneous emergence of multidrug-resistant *Candida auris* on 3 continents confirmed by whole-genome sequencing and epidemiological analyses. *Clinical Infectious Diseases* **64**, 134–140 (2017).

14. Gifford, H., Rhodes, J. & Farrer, R. A. The diverse genomes of *Candida auris*. *The Lancet Microbe* **0**, (2024).

15. Chen, J. *et al.* Is the superbug fungus really so scary? A systematic review and meta-analysis of global epidemiology and mortality of *Candida auris*. *BMC Infectious Diseases* **20**, 827 (2020).

16. Mayer, F. L., Wilson, D. & Hube, B. *Candida albicans* pathogenicity mechanisms. *Virulence* **4**, 119–128 (2013).

17. Phan, Q. T. *et al.* Als3 is a *Candida albicans* invasin that binds to cadherins and induces endocytosis by host cells. *PLOS Biology* **5**, e64 (2007).

18. Moyes, D. L. *et al.* Candidalysin is a fungal peptide toxin critical for mucosal infection. *Nature* **532**, 64–68 (2016).

19. Yue, H. *et al.* Filamentation in *Candida auris*, an emerging fungal pathogen of humans: Passage through the mammalian body induces a heritable phenotypic switch. *Emerging Microbes & Infections* **7**, 1–13 (2018).

20. Chadwick, C., Jesus, M. D., Ginty, F. & Martinez, J. S. Pathobiology of *Candida auris* infection analyzed by multiplexed imaging and single cell analysis. *PLOS ONE* **19**, e0293011 (2024).

21. Santana, D. J. *et al.* A *Candida auris*-specific adhesin, Scf1, governs surface association, colonization, and virulence. *Science* **381**, 1461–1467 (2023).

22. Pelletier, C., Shaw, S., Alsayegh, S., Brown, A. J. P. & Lorenz, A. *Candida auris* undergoes adhesin-dependent and -independent cellular aggregation. *PLOS Pathogens* **20**, e1012076 (2024).

23. Muñoz, J. F. *et al.* Genomic insights into multidrug-resistance, mating and virulence in *Candida auris* and related emerging species. *Nature Communications* **9**, 5346 (2018).

24. Richardson, J. P. *et al.* Candidalysins are a new family of cytolytic fungal peptide toxins. *mBio* **13**, e03510–21 (2022).

25. Horton, M. V. *et al.* *Candida auris* cell wall mannosylation contributes to neutrophil evasion through pathways divergent from *Candida albicans* and *Candida glabrata*. *mSphere* **6**, e00406–21 (2021).

26. Kim, J.-S., Lee, K.-T. & Bahn, Y.-S. Secreted aspartyl protease 3 regulated by the Ras/cAMP/PKA pathway promotes the virulence of *Candida auris*. *Frontiers in Cellular and Infection Microbiology* **13**, 1257897 (2023).

27. Weerasinghe, H. *et al.* *Candida auris* uses metabolic strategies to escape and kill macrophages while avoiding robust activation of the NLRP3 inflammasome response. *Cell Reports* **42**, 112522 (2023).

28. Byun, S. A. *et al.* Virulence traits and azole resistance in Korean *Candida auris* Isolates. *Journal of Fungi* **9**, 979 (2023).

29. Santana, D. J., Zhao, G. & O'Meara, T. R. The many faces of *Candida auris*: Phenotypic and strain variation in an emerging pathogen. *PLOS Pathogens* **20**, e1012011 (2024).

30. Allert, S. *et al.* From environmental adaptation to host survival: Attributes that mediate pathogenicity of *Candida auris*. *Virulence* **13**, 191–214 (2022).

31. Fayed, B. *et al.* Transcriptome analysis of human dermal cells infected with *Candida auris* identified unique pathogenesis/defensive mechanisms particularly ferroptosis. *Mycopathologia* **189**, 65 (2024).

32. Yang, B. *et al.* A correlative study of the genomic underpinning of virulence traits and drug tolerance of *Candida auris*. *Infection and Immunity* **0**, e00103–24 (2024).

33. Bruno, M. *et al.* Transcriptional and functional insights into the host immune response against the emerging fungal pathogen *Candida auris*. *Nature Microbiology* **5**, 1516–1531 (2020).

34. Wang, Y. *et al.* Innate immune responses against the fungal pathogen *Candida auris*. *Nature Communications* **13**, 3553 (2022).

35. Chybowska, A. D., Childers, D. S. & Farrer, R. A. Nine things genomics can tell us about *Candida auris*. *Frontiers in Genetics* **11**, 351 (2020).

36. Wang, X. *et al.* The first isolate of *Candida auris* in China: Clinical and biological aspects. *Emerging Microbes & Infections* **7**, 1–9 (2018).

37. Fan, S., Li, C., Bing, J., Huang, G. & Du, H. Discovery of the diploid form of the emerging fungal pathogen *Candida auris*. *ACS Infectious Diseases* **6**, 2641–2646 (2020).

38. Fan, S. *et al.* A biological and genomic comparison of a drug-resistant and a drug-susceptible strain of *Candida auris* isolated from Beijing, China. *Virulence* **12**, 1388–1399 (2021).

39. Wurster, S., Albert, N. D. & Kontoyiannis, D. P. *Candida auris* bloodstream infection induces upregulation of the PD-1/PD-L1 immune checkpoint pathway in an immunocompetent mouse model. *mSphere* **7**, e00817–21 (2022).

40. Bing, J. *et al.* Rapid evolution of an adaptive multicellular morphology of *Candida auris* during systemic infection. *Nature Communications* **15**, 2381 (2024).

41. Ben-Ami, R. *et al.* Multidrug-resistant *Candida haemulonii* and *C. auris*, Tel Aviv, Israel. *Emerging Infectious Diseases* **23**, (2017).

42. Hager, C. L., Larkin, E. L., Long, L. A. & Ghannoum, M. A. Evaluation of the efficacy of rezafungin, a novel echinocandin, in the treatment of disseminated *Candida auris* infection using an immunocompromised mouse model. *Journal of Antimicrobial Chemotherapy* **73**, 2085–2088 (2018).

43. Zhao, M. *et al.* *In Vivo* Pharmacokinetics and pharmacodynamics of APX001 against *Candida* spp. In a neutropenic disseminated candidiasis mouse model. *Antimicrobial Agents and Chemotherapy* **62**, e02542–17 (2018).

44. Singh, S. *et al.* The NDV-3A vaccine protects mice from multidrug resistant *Candida auris* infection. *PLOS Pathogens* **15**, e1007460 (2019).

45. Zhang, F. *et al.* A marine microbiome antifungal targets urgent-threat drug-resistant fungi. *Science* **370**, 974–978 (2020).

46. Muñoz, J. E. *et al.* Pathogenicity levels of Colombian strains of *Candida auris* and Brazilian strains of *Candida haemulonii* species complex in both murine and*Galleria mellonella* experimental models. *Journal of Fungi* **6**, 104 (2020).

47. Abe, M. *et al.* Potency of gastrointestinal colonization and virulence of *Candida auris* in a murine endogenous candidiasis. *PLoS One* **15**, e0243223 (2020).

48. Forgács, L. *et al.* Comparison of in vivo pathogenicity of four *Candida auris* clades in a neutropenic bloodstream infection murine model. *Emerging Microbes & Infections* **9**, 1160–1169 (2020).

49. Nagy, F. *et al.* In vitro and in vivo interaction of caspofungin with isavuconazole against *Candida auris* planktonic cells and biofilms. *Medical Mycology* **59**, 1015–1023 (2021).

50. Forgács, L. *et al.* In vivo efficacy of amphotericin B against four *Candida auris* Clades. *Journal of Fungi (Basel, Switzerland)* **8**, 499 (2022).

51. Singh, S. *et al.* Protective efficacy of anti-Hyr1p monoclonal antibody against systemic candidiasis due to multi-drug-resistant *Candida auris*. *Journal of Fungi* **9**, 103 (2023).

52. Salama, E. A. *et al.* Lansoprazole interferes with fungal respiration and acts synergistically with amphotericin B against multidrug-resistant *Candida auris*. *Emerging Microbes & Infections* **13**, 2322649 (2024).

53. Torres, S. R. *et al.* Impact of *Candida auris* infection in a neutropenic murine model. *Antimicrobial Agents and Chemotherapy* **64**, e01625–19 (2020).

54. Xin, H., Mohiuddin, F., Tran, J., Adams, A. & Eberle, K. Experimental mouse models of disseminated *Candida auris* infection. *mSphere* **4**, e00339–19 (2019).

55. Rosario-Colon, J., Eberle, K., Adams, A., Courville, E. & Xin, H. *Candida* cell-surface-specific monoclonal antibodies protect mice against *Candida auris* invasive infection. *International Journal of Molecular Sciences* **22**, 6162 (2021).

56. Torres, S. R. *et al.* Assessment of environmental and occupational exposure while working with multidrug resistant (MDR) fungus *Candida auris* in an animal facility. *Journal of Occupational and Environmental Hygiene* **16**, 507–518 (2019).

57. Borman, A. M. Of mice and men and larvae: *Galleria mellonella* to model the early host-pathogen interactions after fungal infection. *Virulence* **9**, 9–12 (2017).

58. Romera, D. *et al.* The *Galleria mellonella* infection model as a system to investigate the virulence of *Candida auris* strains. *Pathogens and Disease* **78**, ftaa067 (2020).

59. García-Carnero, L. C. *et al.* Early virulence predictors during the *Candida* species–*Galleria mellonella* interaction. *Journal of Fungi* **6**, 152 (2020).

60. Garcia-Bustos, V. *et al.* Characterization of the differential pathogenicity of *Candida auris* in a *Galleria mellonella* infection model. *Microbiology Spectrum* **9**, e00013–21 (2021).

61. Carvajal, S. K. *et al.* Pathogenicity assessment of Colombian strains of *Candida auris* in the *Galleria mellonella* invertebrate model. *Journal of Fungi* **7**, 401 (2021).

62. Hernando-Ortiz, A. *et al.* Virulence of *Candida auris* from different clinical origins in *Caenorhabditis elegans* and *Galleria mellonella* host models. *Virulence* **12**, 1063–1075 (2021).

63. Spettel, K. *et al.* *Candida auris* in Austria—what is new and what is different. *Journal of Fungi* **9**, 129 (2023).

64. Wurster, S. *et al.* *Drosophila melanogaster* as a model to study virulence and azole treatment of the emerging pathogen *Candida auris*. *Journal of Antimicrobial Chemotherapy* **74**, 1904–1910 (2019).

65. Harpf, V., Rambach, G., Würzner, R., Lass-Flörl, C. & Speth, C. *Candida* and complement: New aspects in an old battle. *Frontiers in Immunology* **11**, 1471 (2020).

66. Pechacek, J. & Lionakis, M. S. Host defense mechanisms against *Candida auris*. *Expert Review of Anti-infective Therapy* **21**, 1087–1096 (2023).

67. Arora, P. *et al.* Environmental isolation of *Candida auris* from the coastal wetlands of Andaman Islands, India. *mBio* **12**, e03181–20 (2021).

68. Escandón, P. Novel environmental niches for *Candida auris*: Isolation from a coastal habitat in Colombia. *Journal of Fungi* **8**, 748 (2022).

69. Uden, V. & Kolipinski, M. C. *Torulopsis haemulonii nov. spec.*, A yeast from the Atlantic Ocean. *Antonie Van Leeuwenhoek* **28**, 78–80 (1962).

70. Bavia, L., Santiesteban-Lores, L. E., Carneiro, M. C. & Prodocimo, M. M. Advances in the complement system of a teleost fish, *Oreochromis niloticus*. *Fish & Shellfish Immunology* **123**, 61–74 (2022).

71. Buchmann, K., Karami, A. M. & Duan, Y. The early ontogenetic development of immune cells and organs in teleosts. *Fish & Shellfish Immunology* **146**, 109371 (2024).

72. Tian, H. *et al.* Cytokine networks provide sufficient evidence for the differentiation of CD4+ T cells in teleost fish. *Developmental & Comparative Immunology* **141**, 104627 (2023).

73. Johnson, C. J., Davis, J. M., Huttenlocher, A., Kernien, J. F. & Nett, J. E. Emerging fungal pathogen *Candida auris* evades neutrophil attack. *mBio* **9**, e01403–18 (2018).

74. Pharkjaksu, S., Boonmee, N., Mitrpant, C. & Ngamskulrungroj, P. Immunopathogenesis of Emerging *Candida auris* and *Candida haemulonii* Strains. *Journal of Fungi* **7**, 725 (2021).

75. Shapiro, R. S. & Cowen, L. E. Uncovering cellular circuitry controlling temperature-dependent fungal morphogenesis. *Virulence* **3**, 400–404 (2012).

76. Leach, M. D. *et al.* Hsf1 and Hsp90 orchestrate temperature-dependent global transcriptional remodelling and chromatin architecture in *Candida albicans*. *Nature Communications* **7**, 11704 (2016).

77. Xiao, W. *et al.* Response and regulatory mechanisms of heat resistance in pathogenic fungi. *Applied Microbiology and Biotechnology* **106**, 5415–5431 (2022).

78. Akbarzadeh, A. & Leder, E. H. Acclimation of killifish to thermal extremes of hot spring: Transcription of gonadal and liver heat shock genes. *Comparative Biochemistry and Physiology Part A: Molecular & Integrative Physiology* **191**, 89–97 (2016).

79. Hamied, A. *et al.* Identification and characterization of highly fluorescent pigment cells in embryos of the Arabian killifish (*Aphanius Dispar*). *iScience* **23**, 101674 (2020).

80. Alsakran, A. *et al.* Stage-by-stage exploration of normal embryonic development in the Arabian killifish, Aphanius dispar. *Developmental Dynamics* **n/a**, (2024).

81. Minhas, R. *et al.* The thermotolerant Arabian killifish, Aphanius dispar, as a novel infection model for human fungal pathogens. 2024.10.08.617174 (2024) doi:10.1101/2024.10.08.617174.

82. Skrzypek, M. S. *et al.* The Candida Genome Database (CGD): Incorporation of Assembly 22, systematic identifiers and visualization of high throughput sequencing data. *Nucleic Acids Research* **45**, D592–D596 (2017).

83. Potrykus, J. *et al.* Fungal iron availability during deep seated candidiasis is defined by a complex interplay involving systemic and local events. *PLOS pathogens* **9**, e1003676 (2013).

84. Kasper, L. *et al.* The fungal peptide toxin Candidalysin activates the NLRP3 inflammasome and causes cytolysis in mononuclear phagocytes. *Nature Communications* **9**, 4260 (2018).

85. Bonzi, L. C. *et al.* The time course of molecular acclimation to seawater in a euryhaline fish. *Scientific Reports* **11**, 18127 (2021).

86. Varma, A. *et al.* Molecular cloning and functional characterisation of a glucose transporter, CaHGT1, of Candida albicans. *FEMS microbiology letters* **182**, 15–21 (2000).

87. Luo, L., Tong, X. & Farley, P. C. The *Candida albicans* gene HGT12 (Orf19.7094) encodes a hexose transporter. *FEMS Immunology & Medical Microbiology* **51**, 14–17 (2007).

88. Brown, V., Sexton, J. A. & Johnston, M. A glucose sensor in Candida albicans. *Eukaryotic Cell* **5**, 1726–1737 (2006).

89. Larcombe, D. E. *et al.* Glucose-enhanced oxidative stress resistance-A protective anticipatory response that enhances the fitness of *Candida albicans* during systemic infection. *PLOS Pathogens* **19**, e1011505 (2023).

90. Martin, R. *et al.* A core filamentation response network in *Candida albicans* is restricted to eight genes. *PLOS ONE* **8**, e58613 (2013).

91. Schatzman, S. S. *et al.* Copper-only superoxide dismutase enzymes and iron starvation stress in Candida fungal pathogens. *The Journal of Biological Chemistry* **295**, 570–583 (2020).

92. Rybak, J. M. *et al.* Abrogation of Triazole Resistance upon Deletion of *CDR1* in a Clinical Isolate of *Candida auris*. *Antimicrobial Agents and Chemotherapy* **63**, (2019).

93. Li, J., Coste, A. T., Bachmann, D., Sanglard, D. & Lamoth, F. Deciphering the Mrr1/Mdr1 Pathway in Azole Resistance of *Candida auris*. *Antimicrobial Agents and Chemotherapy* **66**, e00067–22 (2022).

94. Sun, S., Coelho, M. A., David-Palma, M., Priest, S. J. & Heitman, J. The evolution of sexual reproduction and the Mating-type locus: Links to pathogenesis of *Cryptococcus* human pathogenic fungi. *Annual Review of Genetics* **53**, 417–444 (2019).

95. Wang, Y. & Xu, J. Population genomic analyses reveal evidence for limited recombination in the superbug *Candida auris* in nature. *Computational and Structural Biotechnology Journal* **20**, 3030–3040 (2022).

96. Overy, D. P., Rämä, T., Oosterhuis, R., Walker, A. K. & Pang, K.-L. The neglected marine fungi, *Sensu stricto*, and their isolation for natural products' discovery. *Marine Drugs* **17**, 42 (2019).

97. Chow, N. A. *et al.* Potential fifth clade of *Candida auris,* Iran, 2018. *Emerging Infectious Diseases* **25**, 1780–1781 (2019).

98. Louvet, M. *et al.* Ume6-dependent pathways of morphogenesis and biofilm formation in *Candida auris*. *Microbiology Spectrum* **0**, e01531–24 (2024).

99. Deng, Y., Li, S., Bing, J., Liao, W. & Tao, L. Phenotypic switching and filamentation in *Candida haemulonii*, an emerging opportunistic pathogen of humans. *Microbiology Spectrum* **9**, e00779–21 (2021).

100. Seiser, S. *et al.* Native human and mouse skin infection models to study *Candida auris*-host interactions. *Microbes and Infection* **26**, 105234 (2024).

101. Fan, S. *et al.* Filamentous growth is a general feature of *Candida auris* clinical isolates. *Medical Mycology* **59**, 734–740 (2021).

102. Bravo Ruiz, G., Ross, Z. K., Gow, N. A. R. & Lorenz, A. Pseudohyphal growth of the emerging pathogen *Candida auris* is triggered by genotoxic stress through the S phase checkpoint. *mSphere* **5**, e00151–20 (2020).

103. Kim, S. H. *et al.* Genetic analysis of *Candida auris* implicates Hsp90 in morphogenesis and azole tolerance and Cdr1 in Azole Resistance. *mBio* **10**, e02529–18 (2019).

104. Gao, J. *et al.* LncRNA DINOR is a virulence factor and global regulator of stress responses in *Candida auris*. *Nature Microbiology* **6**, 842–851 (2021).

105. Ismail, A., Bedell, G. W. & Lupan, D. M. Siderophore production by the pathogenic yeast, *Candida albicans*. *Biochemical and Biophysical Research Communications* **130**, 885–891 (1985).

106. Heymann, P. *et al.* The Siderophore iron transporter of *Candida albicans* (Sit1p/Arn1p) mediates uptake of ferrichrome-type siderophores and Is required for epithelial invasion. *Infection and Immunity* **70**, 5246–5255 (2002).

107. Boiteau, R. M. *et al.* Siderophore-based microbial adaptations to iron scarcity across the eastern Pacific Ocean. *Proceedings of the National Academy of Sciences* **113**, 14237–14242 (2016).

108. Park, J. *et al.* Siderophore production and utilization by marine bacteria in the North Pacific Ocean. *Limnology and Oceanography* **68**, 1636–1653 (2023).

109. Renshaw, J. C. *et al.* Fungal siderophores: Structures, functions and applications. *Mycological Research* **106**, 1123–1142 (2002).

110. Johnstone, T. C. & Nolan, E. M. Beyond iron: Non-classical biological functions of bacterial siderophores. *Dalton Transactions* **44**, 6320–6339 (2015).

111. Nakajima, Y. *et al.* Effect of disrupting the trichothecene efflux pump encoded by *FgTri12* in the nivalenol chemotype of *Fusarium graminearum*. *The Journal of General and Applied Microbiology* **61**, 93–96 (2015).

112. Xue, P. *et al.* Heme sensing and trafficking in fungi. *Fungal Biology Reviews* **43**, 100286 (2023).

113. Fourie, R., Kuloyo, O. O., Mochochoko, B. M., Albertyn, J. & Pohl, C. H. Iron at the Centre of *Candida albicans* Interactions. *Frontiers in Cellular and Infection Microbiology* **8**, 185 (2018).

114. Alselami, A. & Drummond, R. A. How metals fuel fungal virulence, yet promote anti-fungal immunity. *Disease Models & Mechanisms* **16**, dmm050393 (2023).

115. Pradhan, A. *et al.* Non-canonical signalling mediates changes in fungal cell wall PAMPs that drive immune evasion. *Nature Communications* **10**, 5315 (2019).

116. Weissman, Z. & Kornitzer, D. A family of *Candida* cell surface haem-binding proteins involved in haemin and haemoglobin-iron utilization. *Molecular Microbiology* **53**, 1209–1220 (2004).

117. Ding, C. *et al.* Conserved and divergent roles of Bcr1 and CFEM proteins in *Candida parapsilosis and Candida albicans*. *PLOS ONE* **6**, e28151 (2011).

118. Simm, C. *et al.* Disruption of iron homeostasis and mitochondrial metabolism are promising targets to inhibit *Candida auris*. *Microbiology Spectrum* **10**, e00100–22 (2022).

119. Sert, N. P. du *et al.* Reporting animal research: Explanation and elaboration for the ARRIVE guidelines 2.0. *PLOS Biology* **18**, e3000411 (2020).

120. Benjamini, Y. & Hochberg, Y. Controlling the false discovery rate: A practical and powerful approach to multiple testing. *Journal of the Royal Statistical Society Series B: Statistical Methodology* **57**, 289–300 (1995).

121. Bancroft, J. & Stevens, A. Theory and Practice of Histological Techniques. (1977).

122. Chen, S., Zhou, Y., Chen, Y. & Gu, J. Fastp: An ultra-fast all-in-one FASTQ preprocessor. *Bioinformatics* **34**, i884–i890 (2018).

123. Ewels, P., Magnusson, M., Lundin, S. & Käller, M. MultiQC: Summarize analysis results for multiple tools and samples in a single report. *Bioinformatics* **32**, 3047–3048 (2016).

124. Haas, B. J. *et al.* De novo transcript sequence reconstruction from RNA-seq using the Trinity platform for reference generation and analysis. *Nature Protocols* **8**, 1494–1512 (2013).

125. Abastabar, M. *et al.* *Candida auris* otomycosis in Iran and review of recent literature. *Mycoses* **62**, 101–105 (2019).

126. Muñoz, J. F. *et al.* Clade-specific chromosomal rearrangements and loss of subtelomeric adhesins in *Candida auris*. *Genetics* **218**, iyab029 (2021).

127. Langmead, B. & Salzberg, S. L. Fast gapped-read alignment with Bowtie 2. *Nature Methods* **9**, 357–359 (2012).

128. Li, B. & Dewey, C. N. RSEM: Accurate transcript quantification from RNA-Seq data with or without a reference genome. *BMC Bioinformatics* **12**, 323 (2011).

129. Robinson, M. D., McCarthy, D. J. & Smyth, G. K. edgeR: A Bioconductor package for differential expression analysis of digital gene expression data. *Bioinformatics* **26**, 139–140 (2010).

130. Li, H. *et al.* The Sequence Alignment/Map format and SAMtools. *Bioinformatics* **25**, 2078–2079 (2009).

131. Ritchie, M. E. *et al.* Limma powers differential expression analyses for RNA-sequencing and microarray studies. *Nucleic Acids Research* **43**, e47 (2015).

132. Gu, Z., Eils, R. & Schlesner, M. Complex heatmaps reveal patterns and correlations in multidimensional genomic data. *Bioinformatics* **32**, 2847–2849 (2016).

133. Ashburner, M. *et al.* Gene Ontology: Tool for the unification of biology. *Nature Genetics* **25**, 25–29 (2000).

134. The Gene Ontology Consortium *et al.* The Gene Ontology knowledgebase in 2023. *Genetics* **224**, iyad031 (2023).

135. Buchfink, B., Reuter, K. & Drost, H.-G. Sensitive protein alignments at tree-of-life scale using DIAMOND. *Nature Methods* **18**, 366–368 (2021).

136. Golden, C., Studholme, D. J. & Farrer, R. A. DIAMOND2GO: A rapid Gene Ontology assignment and enrichment tool for functional genomics. 2024.08.19.608700 (2024) doi:10.1101/2024.08.19.608700.

137. Kanehisa, M., Furumichi, M., Sato, Y., Kawashima, M. & Ishiguro-Watanabe, M. KEGG for taxonomy-based analysis of pathways and genomes. *Nucleic Acids Research* **51**, D587–D592 (2022).

138. Kanehisa, M., Sato, Y. & Morishima, K. BlastKOALA and GhostKOALA: KEGG tools for functional characterization of genome and metagenome sequences. *Journal of Molecular Biology* **428**, 726–731 (2016).

139. Bateman, A. *et al.* The Pfam protein families database. *Nucleic Acids Research* **32**, D138–D141 (2004).

140. Eddy, S. R. Accelerated Profile HMM Searches. *PLOS Computational Biology* **7**, e1002195 (2011).

141. Almagro Armenteros, J. J. *et al.* SignalP 5.0 improves signal peptide predictions using deep neural networks. *Nature Biotechnology* **37**, 420–423 (2019).

142. Hallgren, J. *et al.* DeepTMHMM predicts alpha and beta transmembrane proteins using deep neural networks. (2022) doi:10.1101/2022.04.08.487609.

143. Gíslason, M. H., Nielsen, H., Almagro Armenteros, J. J. & Johansen, A. R. Prediction of GPI-anchored proteins with pointer neural networks. *Current Research in Biotechnology* **3**, 6–13 (2021).

144. Camacho, C. *et al.* BLAST+: Architecture and applications. *BMC Bioinformatics* **10**, 421 (2009).

145. Supek, F., Bošnjak, M., Škunca, N. & Šmuc, T. REVIGO summarizes and visualizes long lists of gene ontology terms. *PLOS ONE* **6**, e21800 (2011).

146. Farrer, R. A. Synima: A Synteny imaging tool for annotated genome assemblies. *BMC Bioinformatics* **18**, 507 (2017).

147. Emms, D. M. & Kelly, S. OrthoFinder: Phylogenetic orthology inference for comparative genomics. *Genome Biology* **20**, 238 (2019).

148. Edgar, R. C. MUSCLE: Multiple sequence alignment with high accuracy and high throughput. *Nucleic Acids Research* **32**, 1792–1797 (2004).

149. Price, M. N., Dehal, P. S. & Arkin, A. P. FastTree 2 – approximately maximum-likelihood trees for large alignments. *PLOS ONE* **5**, e9490 (2010).

150. Abramson, J. *et al.* Accurate structure prediction of biomolecular interactions with AlphaFold 3. *Nature* **630**, 493–500 (2024).

151. Pettersen, E. F. *et al.* UCSF ChimeraX: Structure visualization for researchers, educators, and developers. *Protein Science* **30**, 70–82 (2021).

152. Stamatakis, A. RAxML version 8: A tool for phylogenetic analysis and post-analysis of large phylogenies. *Bioinformatics* **30**, 1312–1313 (2014).

153. Sievers, F. & Higgins, D. G. Clustal omega. *Current Protocols in Bioinformatics* **48**, 3.13.1–3.13.16 (2014).

End Matter

Acknowledgements

We acknowledge funding from the MRC Centre for Medical Mycology at the University of Exeter (MR/N006364/2, MR/V033417/1), MRC Doctoral Training Grants MR/P501955/2 and MR/W502649/1, Wellcome Trust Career Development Award (215239/Z/19/Z) and Wellcome Trust fellowship (219551/Z/19/Z), National Centre for the Replacement, Refinement and Reduction of Animals in Research (NC3Rs) (NC/X001121/1), and the NIHR Exeter Biomedical Research Centre. TB also was supported *via* Elizabeth Ballou and a Sir Henry Dale Fellowship jointly funded by the Wellcome Trust and the Royal Society (211241/Z/18/Z) and the Lister Institute. The views expressed are those of the authors and not necessarily those of the NIHR or the Department of Health and Social Care. We thank staff in the Aquatic Resource Center

at the University of Exeter for husbandry of the fish and the support for developing protocols for feeding, spawning, and raising new generations of this relatively new model species, including Sam Worthington, Chloe Flint and Richard Silcox. We also thank the Exeter Sequencing Service facility and support from Wellcome Trust Institutional Strategic Support Fund (WT097835MF), Wellcome Trust Multi User Equipment Awards (WT101650MA and 218247/Z/19/Z), Medical Research Council Clinical Infrastructure Funding (MR/M008924/1) and BBSRC LOLA award (BB/K003240/1). We also thank the University of Exeter High-Performance Computing (HPC) facility funded by the UK MRC Clinical Research Infrastructure Initiative (award number MR/M008924/1). We thank Tanmoy Chakraborty, Dhara Malavia and Neil Gow for providing *C. auris* strains, Teigan Veale, Sumita Roy, Jonathan Ball and Darren Thomson for assistance in microscopy and Chloe Pelletier for advice on aggregation. We also thank Microtechnical Services, Exeter, UK, for assistance with histological sectioning.

Author Contributions

HG: designed and conducted experiments, performed analysis, drafted and wrote the paper. NH, JG, QM, TB: optimised, designed or performed experiments. RF, TK, TB, MR, JR, DW, AB: designed experiments, obtained funding. All authors edited the manuscript.

Competing Interests

JR has received honoraria from Gilead for conference presentations. Other authors declare no competing interests.

ORCID IDs

HG (https://orcid.org/0000-0003-2797-852X), TB (https://orcid.org/0000-0002-5315-2759), NH (https://orcid.org/0000-0003-0260-023X), JG (https://orcid.org/0009-0003-3803-9496), QM (https://orcid.org/0000-0001-9892-4997), AB (https://orcid.org/0000-0002-7381-131X), DW (https://orcid.org/0000-0001-6617-0123), JR (https://orcid.org/0000-0002-1338-7860), MR (https://orcid.org/0009-0009-0746-4127), TK (https://orcid.org/0000-0002-5373-2737), RF (https://orcid.org/0000-0001-8456-7458)

Figures

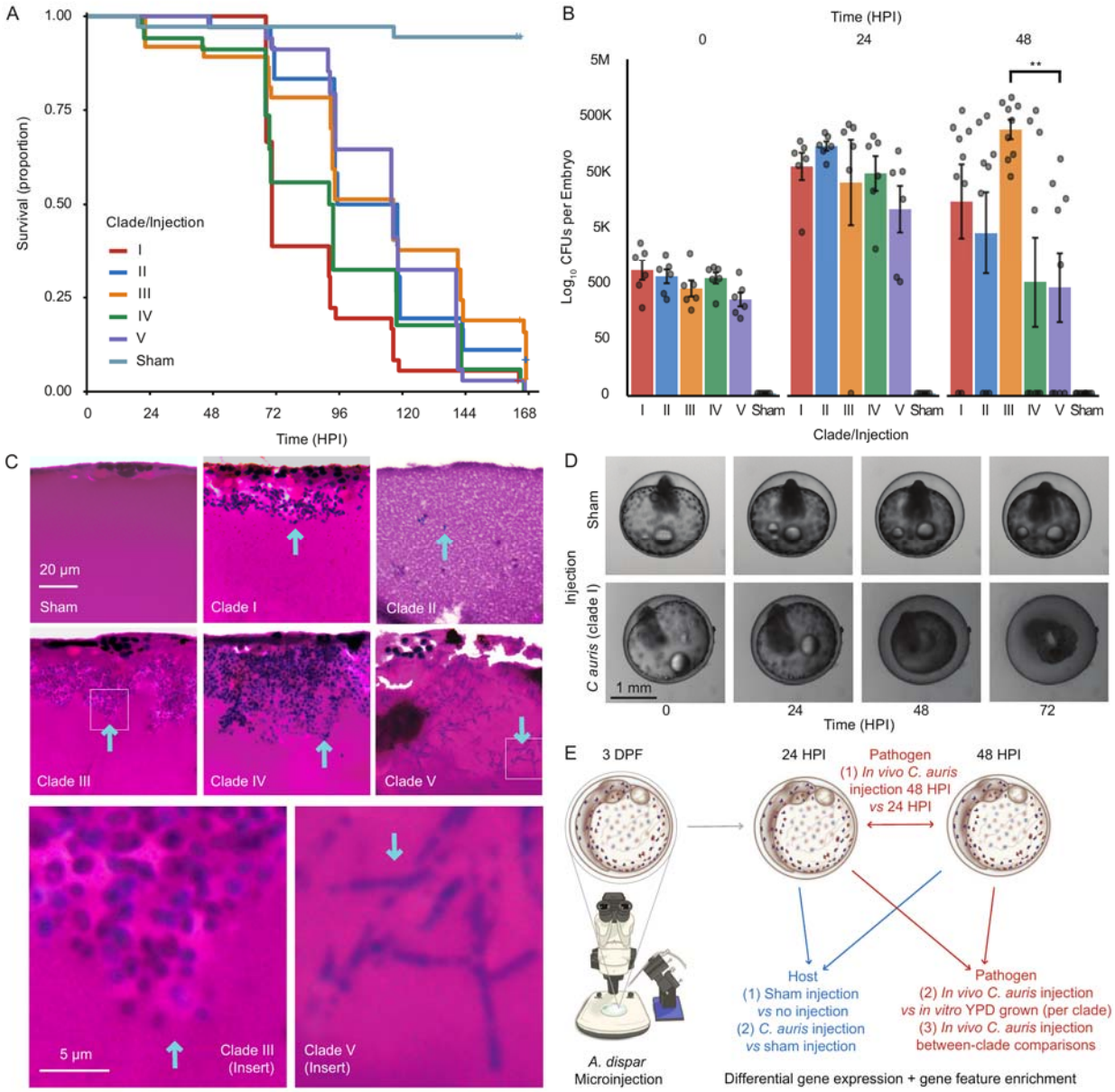

Figure 1. Modelling C. auris infection in the Arabian killifish (A) *Survival curves for embryos injected with each C. auris clade or sham injection. Significance testing between groups is given in* ***Table S1****; hours post injection (HPI).* ***(B)*** *Colony forming units (CFUs) per clade from embryos homogenised after injection as an indicator of*

injection dose and in vivo growth. ***(C)*** *H&E Staining of AK yolk-sac at 48 HPI for each clade or sham injection; morphology is indicated by blue arrows, with insets indicating typical yeast (clade III) and filamentous morphology (clade V). The yolk-sac edge is oriented at the top.* ***(D)*** *Illustrative time-lapse microscopy of embryo death including yolk-sac collapse during infection (clade I infection) or survival (sham injection) using Acquifer live imaging.* ***(E)*** *Experimental scheme for differential gene expression analysis of RNA extracted from AK embryos injected at 3 days post fertilisation (DPF).*

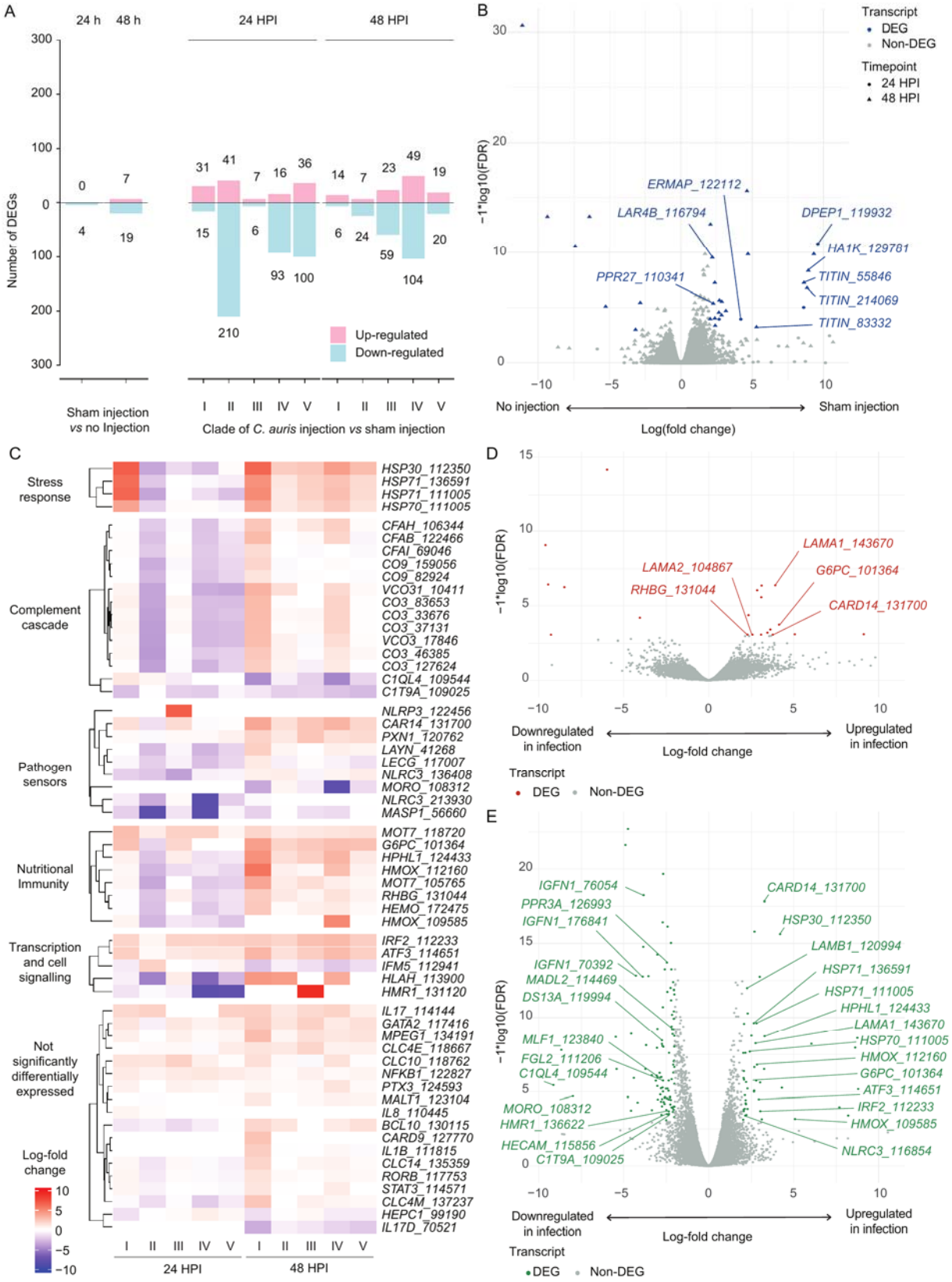
A
24 h
48 h
24 HPI
48 HPI
Number of DEGs
Up-regulated
Down-regulated
Sham injection vs no Injection
Clade of C. auris injection vs sham injection
B
Transcript
DEG
Non-DEG
Timepoint
24 HPI
48 HPI
−1*log10(FDR)
ERMAP_122112
LAR4B_116794
DPEP1_119932
HA1K_129781
PPR27_110341
TITIN_55846
TITIN_214069
TITIN_83332
No injection
Sham injection
Log(fold change)
C
Stress response
Complement cascade
Pathogen sensors
Nutritional Immunity
Transcription and cell signalling
Not significantly differentially expressed
Log-fold change
24 HPI
48 HPI
D
LAMA1_143670
LAMA2_104867
G6PC_101364
RHBG_131044
CARD14_131700
Downregulated in infection
Upregulated in infection
Log-fold change
Transcript
DEG
Non-DEG
E
IGFN1_76054
PPR3A_126993
IGFN1_176841
CARD14_131700
HSP30_112350
LAMB1_120994
IGFN1_70392
MADL2_114469
DS13A_119994
HSP71_136591
HSP71_111005
HPHL1_124433
LAMA1_143670
MLF1_123840
HSP70_111005
FGL2_111206
HMOX_112160
C1QL4_109544
G6PC_101364
ATF3_114651
MORO_108312
IRF2_112233
HMR1_136622
HMOX_109585
HECAM_115856
NLRC3_116854
C1T9A_109025
Downregulated in infection
Upregulated in infection
Log-fold change
Transcript
DEG
Non-DEG

1283

Figure 2. AK host responses to C. auris infection: (A) *Number of differentially expressed genes (DEGs) for each of two comparisons, sham injection vs no injection (left panel), and C. auris injection vs sham injection (right panel), at either 24 or 48 h post injection (HPI).* ***(B)*** *Volcano plot showing log-fold change and significance according to -log^{10} false discovery rate (FDR) for sham injection vs no injection.* ***(C)*** *Heatmap demonstrating log-fold change for differential expression between C. auris injection and sham injection for groups of genes.* ***(D-E)*** *Volcano plots showing log-fold change and significance for DEGs expressed during infection with the two more virulent clades of C. auris at 48 HPI, clade I (**D**, DEGs in red) and clade IV (**E**, DEGs in green).*

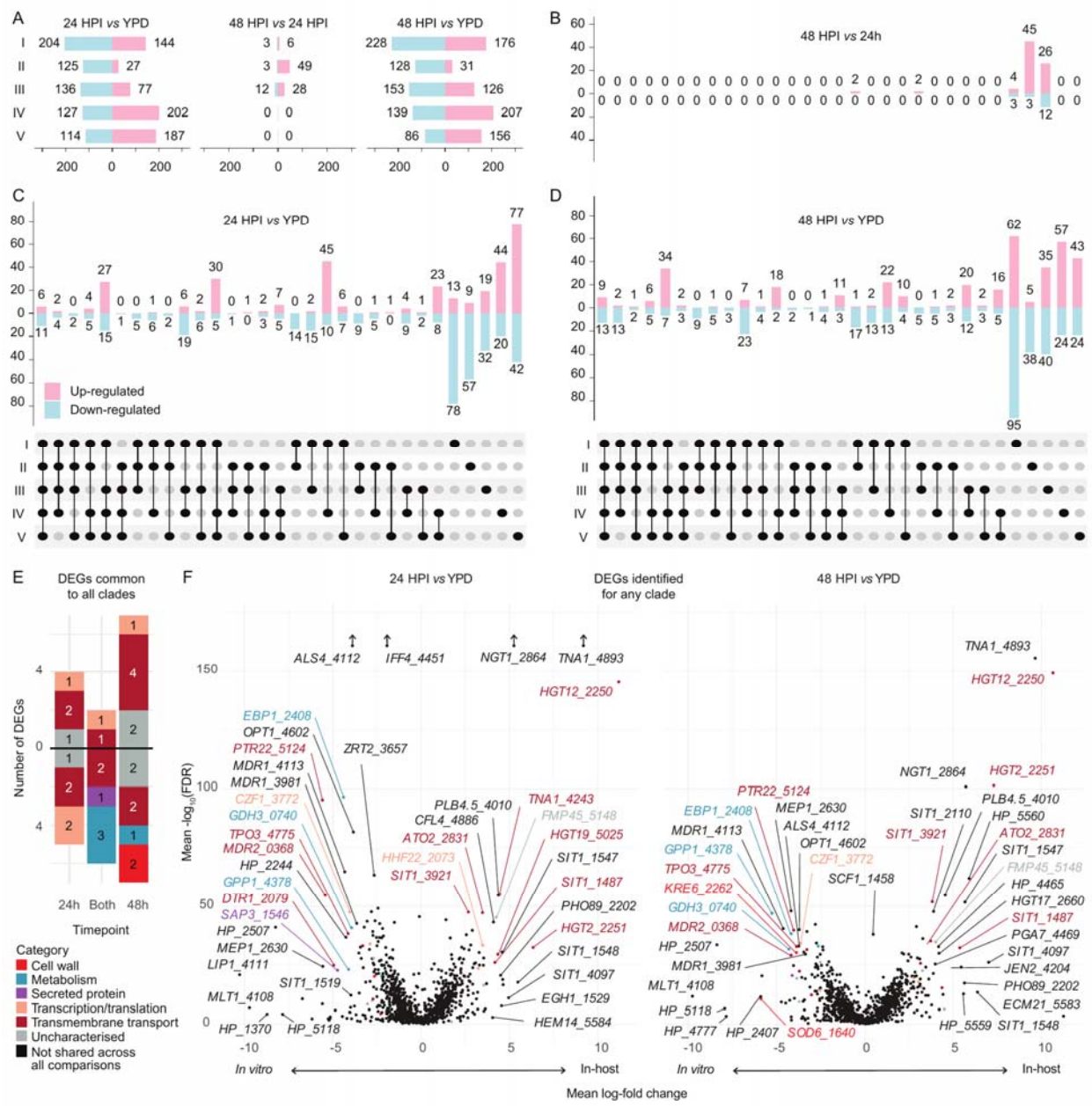

1293

1294 ***Figure 3: C. auris gene expression* in vivo vs in vitro *(A)*** *Total DEGs per clade for*
1295 *each comparison between 24 h post injection (HPI), 48 HPI, and growth in YPD alone.*
1296 ***(B-D)*** *Upset plots for each comparison, indicating DEGs that were significant across all*
1297 *five clades (far left) and for each individual clade (far right) and each set in between.* ***(E)***
1298 *Combined set of significant DEGs common to all five clades between in vivo infection*
1299 *and in vivo growth in YPD. Genes are coloured by manually annotated category* ***(Table***

S4)*. *(F) *Volcano plots demonstrate mean log-fold change for DEGs identified for any clade. Genes with infinite false discovery rate (FDR) are indicated with an arrow. Genes included in the combined set are coloured by category as per panel **E**.*

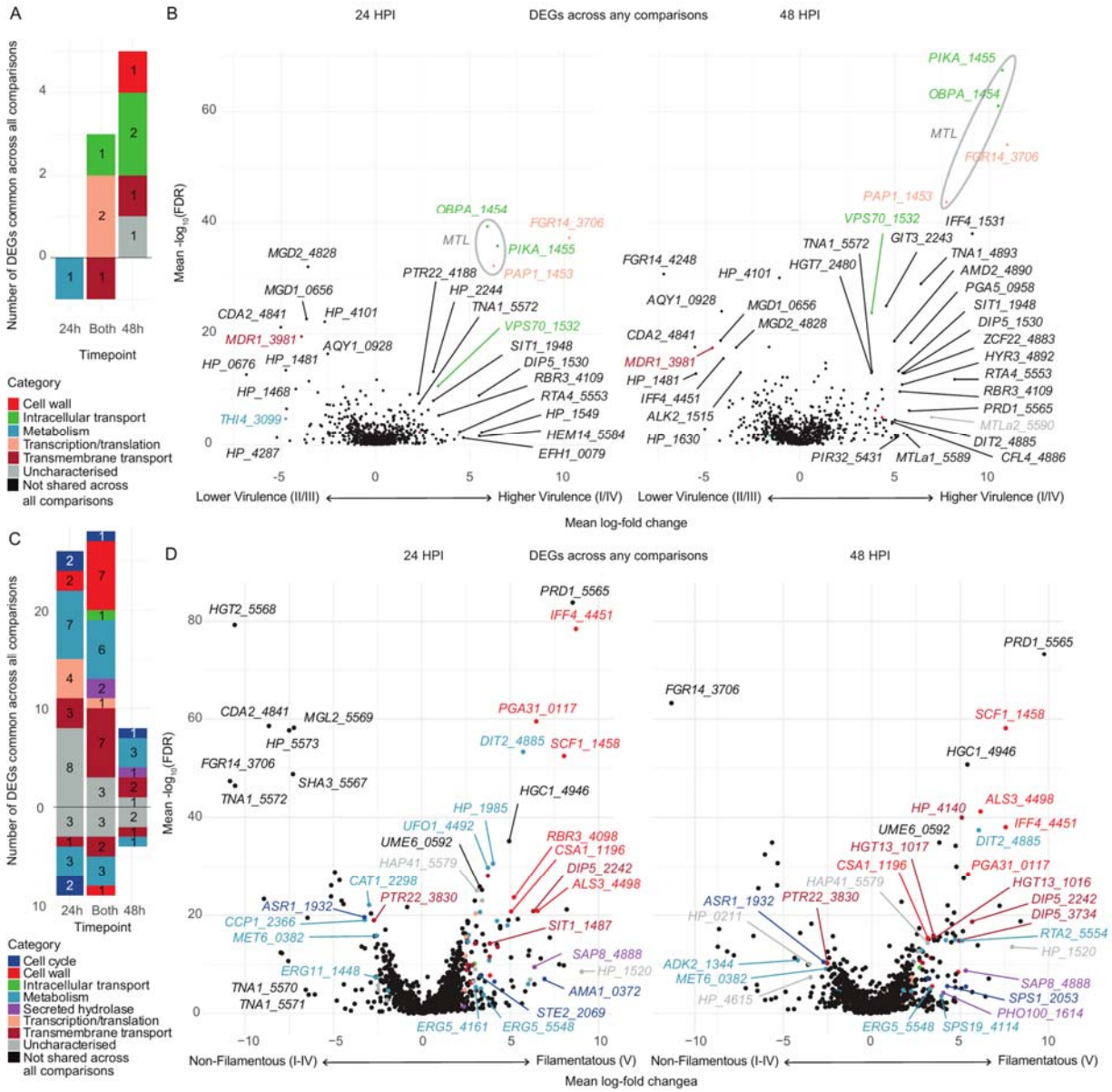

Figure 4: Interclade comparisons for virulence and filamentation: (A): *The set of differentially expressed genes (DEGs) shared across all comparisons between clade I and IV (more virulent) and clade II and III (less virulent), coloured by manually*

annotated category, at either 24 or 48 h post infection (HPI). ***(B)*** *Volcano plots demonstrate mean log-fold change for each DEG found in any comparison; genes included in the combined set are coloured as per* ***A****.* ***(C)*** *The set of DEGs shared across all comparisons between filamenting clade V all other clades (I-IV) in vivo, coloured by manually annotated category.* ***(D):*** *Volcano plots demonstrating mean log-fold change for all comparisons between clade V and clades I-IV at 24 HPI and 48 HPI for each DEG found in any comparison; genes included in the combined set are coloured as per* ***C****.*

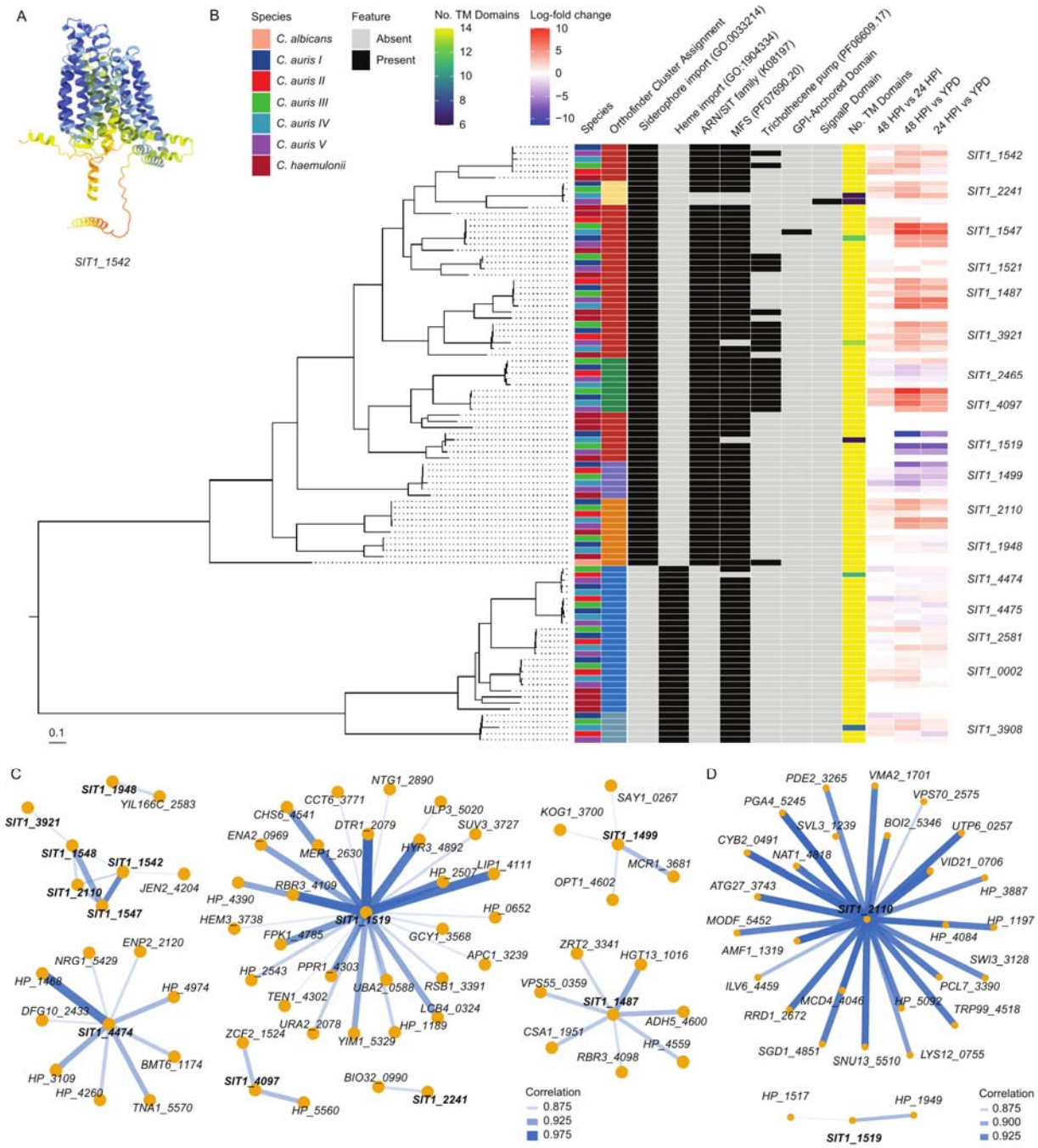

1315

1316 ***Figure 5. Xenosiderophore Transporter Analysis: (A)*** *AlphaFold 3 predicted protein*
1317 *folding for peptide sequences for a xenosiderophore transporter candidate, illustrating*
1318 *the conserved 14-transmembrane domain similarity across the families.* ***(B)*** *RAXML*
1319 *phylogeny using 1000 bootstraps and LG4X model of Muscle-aligned protein*

sequences for orthologues of C. albicans Siderophore Transport 1 SIT1 gene. Scale bar indicates number of substitutions per site. Orthofinder cluster assignment notes which grouping each gene was assigned to by our Synima/Orthofinder pipeline. ***(C)*** *Co-expression network of associated gene expression involving siderophore transport candidate genes.* ***(D)*** *Co-expression network across available RNA-seq data from meta-analysis of 35 studies (****Table S4****), demonstrating a different set of transcriptional networks indicated by external experimental data.*

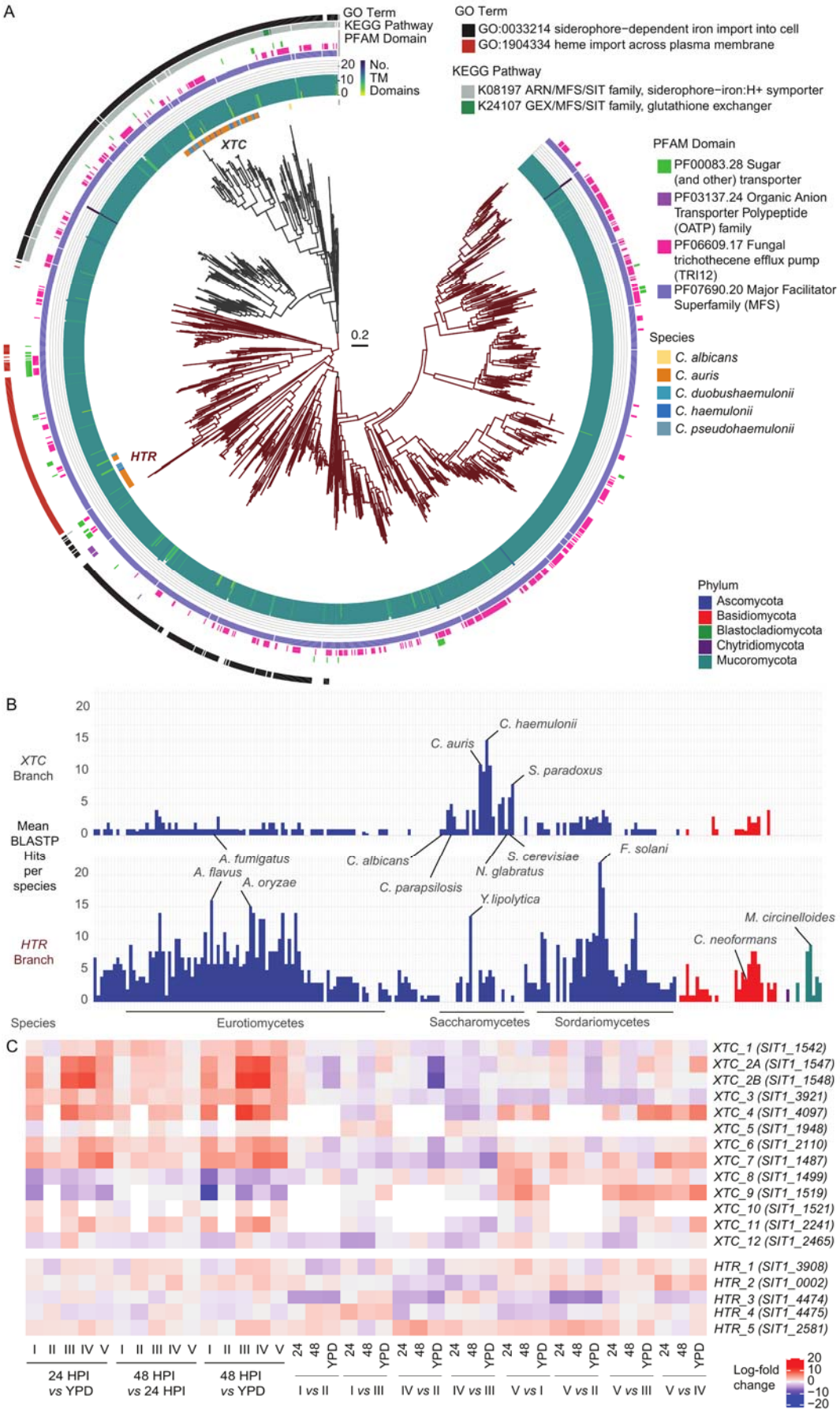
A
GO Term
KEGG Pathway
PFAM Domain
20
10
0
No. TM Domains
XTC
HTR
0.2
GO Term
GO:0033214 siderophore−dependent iron import into cell
GO:1904334 heme import across plasma membrane
KEGG Pathway
K08197 ARN/MFS/SIT family, siderophore−iron:H+ symporter
K24107 GEX/MFS/SIT family, glutathione exchanger
PFAM Domain
PF00083.28 Sugar (and other) transporter
PF03137.24 Organic Anion Transporter Polypeptide (OATP) family
PF06609.17 Fungal trichothecene efflux pump (TRI12)
PF07690.20 Major Facilitator Superfamily (MFS)
Species
C. albicans
C. auris
C. duobushaemulonii
C. haemulonii
C. pseudohaemulonii
Phylum
Ascomycota
Basidiomycota
Blastocladiomycota
Chytridiomycota
Mucoromycota
B
XTC Branch
Mean BLASTP Hits per species
HTR Branch
C. haemulonii
C. auris
S. paradoxus
A. fumigatus
A. flavus
A. oryzae
C. albicans
C. parapsilosis
S. cerevisiae
N. glabratus
Y. lipolytica
F. solani
M. circinelloides
C. neoformans
Species
Eurotiomycetes
Saccharomycetes
Sordariomycetes
C
XTC_1 (SIT1_1542)
XTC_2A (SIT1_1547)
XTC_2B (SIT1_1548)
XTC_3 (SIT1_3921)
XTC_4 (SIT1_4097)
XTC_5 (SIT1_1948)
XTC_6 (SIT1_2110)
XTC_7 (SIT1_1487)
XTC_8 (SIT1_1499)
XTC_9 (SIT1_1519)
XTC_10 (SIT1_1521)
XTC_11 (SIT1_2241)
XTC_12 (SIT1_2465)
HTR_1 (SIT1_3908)
HTR_2 (SIT1_0002)
HTR_3 (SIT1_4474)
HTR_4 (SIT1_4475)
HTR_5 (SIT1_2581)
24 HPI vs YPD
48 HPI vs 24 HPI
48 HPI vs YPD
I vs II
I vs III
IV vs II
IV vs III
V vs I
V vs II
V vs III
V vs IV
Log-fold change
20
10
0
−10
−20

Figure 6. Panfungal Xenosiderophore Phylogeny: (A) *Phylogeny of Blastp hits for C. albicans SIT1 across fungal genomes available in FungiDB. Sequences were aligned with Clustal Omega and FastTree, scale bar shows substitutions per site. Two main branches emerged, a xenosiderophore transporter candidate branch (XTC) and a haem transport-related branch (HTR), based mainly on the GO terms assigned (outer ring).* ***(B)*** *Bar chart depicting per-species mean Blastp hits for siderophore transporters.* ***(C)*** *Heatmap of all DEGs across comparisons in this paper for each XTC and HTR gene, assigned in order of contig in the B8441 v3 reference genome. White spaces represent clades where each orthologue was not found in Orthofinder (XTC4, XTC9 and XTC11 in clade II, XTC5 in II and V, XTC10 in II and IV,* ***Fig. 5B****).*

Supplementary Figures

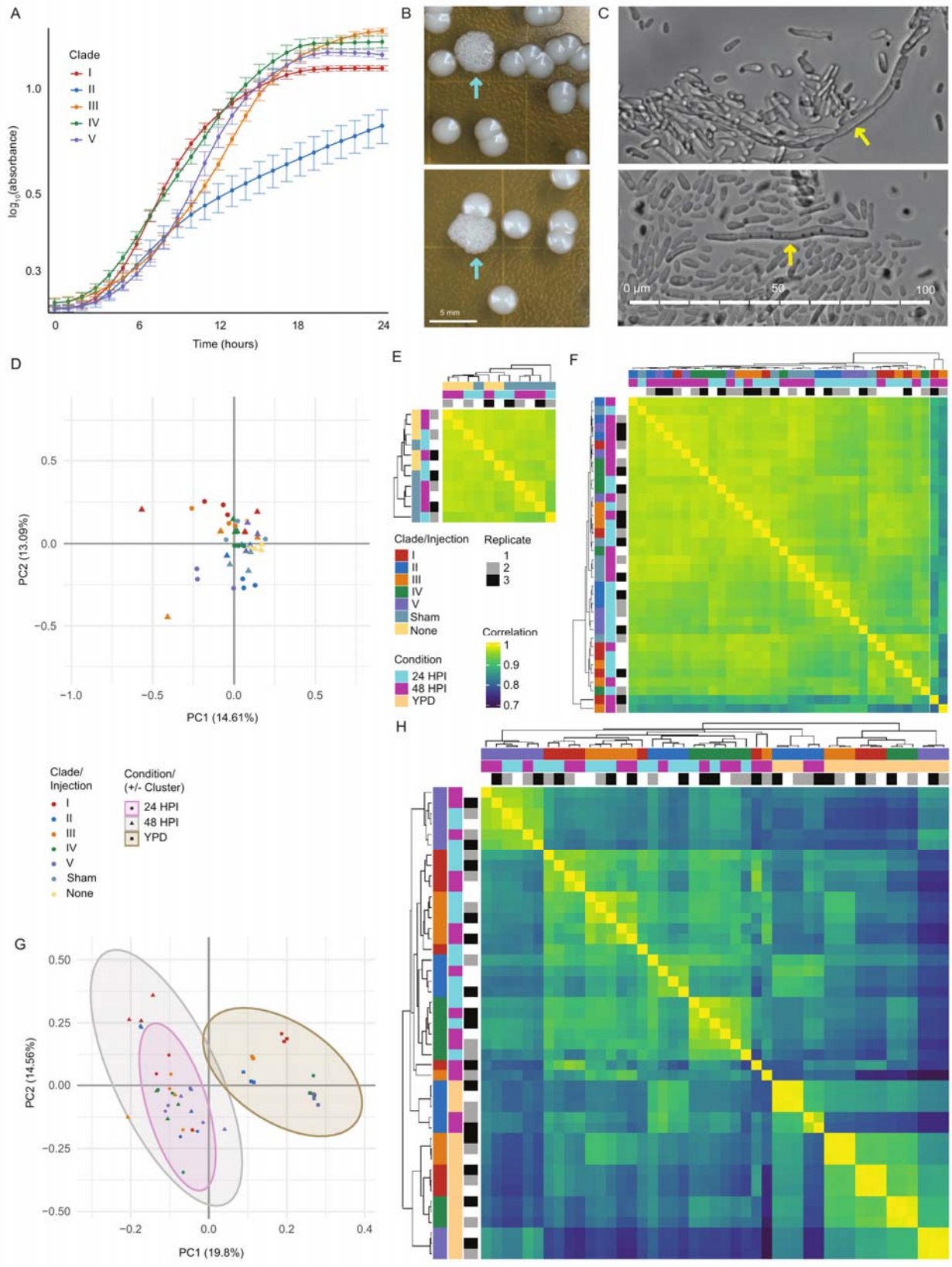
A
Clade
I
II
III
IV
V
log10(absorbance)
Time (hours)
B
5 mm
C
0 µm
50
100
D
PC2 (13.09%)
PC1 (14.61%)
Clade/
Injection
Condition/
(+/- Cluster)
24 HPI
48 HPI
YPD
Sham
None
E
Clade/Injection
Replicate
Condition
Correlation
F
G
PC2 (14.56%)
PC1 (19.8%)
H

1340

Supplementary Figure 1: *Profiles of C. auris growth, morphotype, morphology, and gene expression.* ***(A)*** *Growth curves for five representative strains of C. auris over 24 h in vitro.* ***(B)*** *Rough colonies demonstrated on YPD-agar after recovery from AK infection in clade V only (blue arrows).* ***(C)*** *Filamentous forms (yellow arrows) isolated from rough colonies and imaged on light microscopy in distilled de-ionised water.* ***(D)*** *Principle components analysis (PCA) of fragments per kilobase per million (FPKM) gene expression for AK host transcription.* ***(E)*** *Correlation matrix for individual replicates' log_2-transformed transcript counts per million for AK responses to sham injection and no injection* ***(F)*** *Correlation matrix as above for AK responses to C. auris infection and sham injection.* ***(G)*** *PCA of FPKM gene expression for C. auris pathogen transcription.* ***(H)*** *Correlation matrix as above for C. auris gene expression in vivo and in vivo across five clades.*

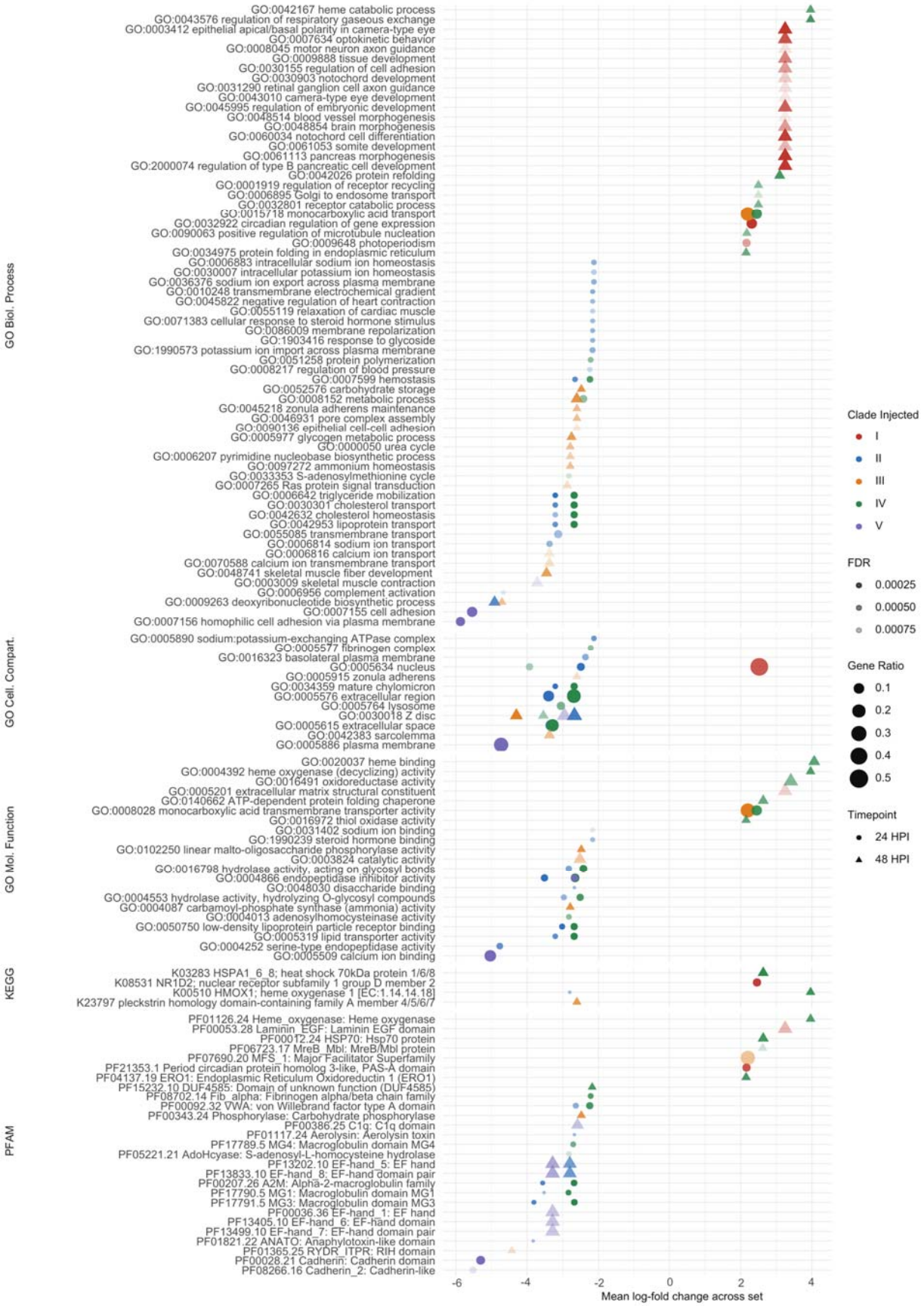
GO Biol. Process
GO:0042167 heme catabolic process
GO:0043576 regulation of respiratory gaseous exchange
GO:0003412 epithelial apical/basal polarity in camera-type eye
GO:0007634 optokinetic behavior
GO:0008045 motor neuron axon guidance
GO:0009888 tissue development
GO:0030155 regulation of cell adhesion
GO:0030903 notochord development
GO:0031290 retinal ganglion cell axon guidance
GO:0043010 camera-type eye development
GO:0045995 regulation of embryonic development
GO:0048514 blood vessel morphogenesis
GO:0048854 brain morphogenesis
GO:0060034 notochord cell differentiation
GO:0061053 somite development
GO:0061113 pancreas morphogenesis
GO:2000074 regulation of type B pancreatic cell development
GO:0042026 protein refolding
GO:0001919 regulation of receptor recycling
GO:0006895 Golgi to endosome transport
GO:0032801 receptor catabolic process
GO:0015718 monocarboxylic acid transport
GO:0032922 circadian regulation of gene expression
GO:0090063 positive regulation of microtubule nucleation
GO:0009648 photoperiodism
GO:0034975 protein folding in endoplasmic reticulum
GO:0006883 intracellular sodium ion homeostasis
GO:0030007 intracellular potassium ion homeostasis
GO:0036376 sodium ion export across plasma membrane
GO:0010248 transmembrane electrochemical gradient
GO:0045822 negative regulation of heart contraction
GO:0055119 relaxation of cardiac muscle
GO:0071383 cellular response to steroid hormone stimulus
GO:0086009 membrane repolarization
GO:1903416 response to glycoside
GO:1990573 potassium ion import across plasma membrane
GO:0051258 protein polymerization
GO:0008217 regulation of blood pressure
GO:0007599 hemostasis
GO:0052576 carbohydrate storage
GO:0008152 metabolic process
GO:0045218 zonula adherens maintenance
GO:0046931 pore complex assembly
GO:0090136 epithelial cell-cell adhesion
GO:0005977 glycogen metabolic process
GO:0000050 urea cycle
GO:0006207 pyrimidine nucleobase biosynthetic process
GO:0097272 ammonium homeostasis
GO:0033353 S-adenosylmethionine cycle
GO:0007265 Ras protein signal transduction
GO:0006642 triglyceride mobilization
GO:0030301 cholesterol transport
GO:0042632 cholesterol homeostasis
GO:0042953 lipoprotein transport
GO:0055085 transmembrane transport
GO:0006814 sodium ion transport
GO:0006816 calcium ion transport
GO:0070588 calcium ion transmembrane transport
GO:0048741 skeletal muscle fiber development
GO:0003009 skeletal muscle contraction
GO:0006956 complement activation
GO:0009263 deoxyribonucleotide biosynthetic process
GO:0007155 cell adhesion
GO:0007156 homophilic cell adhesion via plasma membrane
GO Cell. Compart.
GO:0005890 sodium:potassium-exchanging ATPase complex
GO:0005577 fibrinogen complex
GO:0016323 basolateral plasma membrane
GO:0005634 nucleus
GO:0005915 zonula adherens
GO:0034359 mature chylomicron
GO:0005576 extracellular region
GO:0005764 lysosome
GO:0030018 Z disc
GO:0005615 extracellular space
GO:0042383 sarcolemma
GO:0005886 plasma membrane
GO Mol. Function
GO:0020037 heme binding
GO:0004392 heme oxygenase (decyclizing) activity
GO:0016491 oxidoreductase activity
GO:0005201 extracellular matrix structural constituent
GO:0140662 ATP-dependent protein folding chaperone
GO:0008028 monocarboxylic acid transmembrane transporter activity
GO:0016972 thiol oxidase activity
GO:0031402 sodium ion binding
GO:1990239 steroid hormone binding
GO:0102250 linear malto-oligosaccharide phosphorylase activity
GO:0003824 catalytic activity
GO:0016798 hydrolase activity, acting on glycosyl bonds
GO:0004866 endopeptidase inhibitor activity
GO:0048030 disaccharide binding
GO:0004553 hydrolase activity, hydrolyzing O-glycosyl compounds
GO:0004087 carbamoyl-phosphate synthase (ammonia) activity
GO:0004013 adenosylhomocysteinase activity
GO:0050750 low-density lipoprotein particle receptor binding
GO:0005319 lipid transporter activity
GO:0004252 serine-type endopeptidase activity
GO:0005509 calcium ion binding
KEGG
K03283 HSPA1_6_8; heat shock 70kDa protein 1/6/8
K08531 NR1D2; nuclear receptor subfamily 1 group D member 2
K00510 HMOX1; heme oxygenase 1 [EC:1.14.14.18]
K23797 pleckstrin homology domain-containing family A member 4/5/6/7
PFAM
PF01126.24 Heme_oxygenase: Heme oxygenase
PF00053.28 Laminin_EGF: Laminin EGF domain
PF00012.24 HSP70: Hsp70 protein
PF06723.17 MreB_Mbl: MreB/Mbl protein
PF07690.20 MFS_1: Major Facilitator Superfamily
PF21353.1 Period circadian protein homolog 3-like, PAS-A domain
PF04137.19 ERO1: Endoplasmic Reticulum Oxidoreductin 1 (ERO1)
PF15232.10 DUF4585: Domain of unknown function (DUF4585)
PF08702.14 Fib_alpha: Fibrinogen alpha/beta chain family
PF00092.32 VWA: von Willebrand factor type A domain
PF00343.24 Phosphorylase: Carbohydrate phosphorylase
PF00386.25 C1q: C1q domain
PF01117.24 Aerolysin: Aerolysin toxin
PF17789.5 MG4: Macroglobulin domain MG4
PF05221.21 AdoHcyase: S-adenosyl-L-homocysteine hydrolase
PF13202.10 EF-hand_5: EF hand
PF13833.10 EF-hand_8: EF-hand domain pair
PF00207.26 A2M: Alpha-2-macroglobulin family
PF17790.5 MG1: Macroglobulin domain MG1
PF17791.5 MG3: Macroglobulin domain MG3
PF00036.36 EF-hand_1: EF hand
PF13405.10 EF-hand_6: EF-hand domain
PF13499.10 EF-hand_7: EF-hand domain pair
PF01821.22 ANATO: Anaphylotoxin-like domain
PF01365.25 RYDR_ITPR: RIH domain
PF00028.21 Cadherin: Cadherin domain
PF08266.16 Cadherin_2: Cadherin-like
-6
-4
-2
0
2
4
Mean log-fold change across set
Clade Injected
I
II
III
IV
V
FDR
0.00025
0.00050
0.00075
Gene Ratio
0.1
0.2
0.3
0.4
0.5
Timepoint
24 HPI
48 HPI

1353

Supplementary Figure 2: A. dispar gene ontology, pathway and domain enrichment during infection vs sham control: *The GJEY01 A. dispar transcripts were annotated for Gene Ontology (GO) terms using DIAMOND2GO, Kyoto Encycopaedia of Genes and Genome pathways using BLASTKoala, and PFAM domains using HMMScan. For each set of up-regulated or down-regulated genes in each comparison between an injected C. auris clade and sham injection, Fisher's exact test was used with Benjamini-Hochberg (BH) correction for multiple testing for each set, with a false discovery rate (FDR) cut-off of 0.001. Mean log-fold change and ratio of genes in that set was calculated for genes in each set possessing each feature. Redundant GO terms were removed using Revigo.*

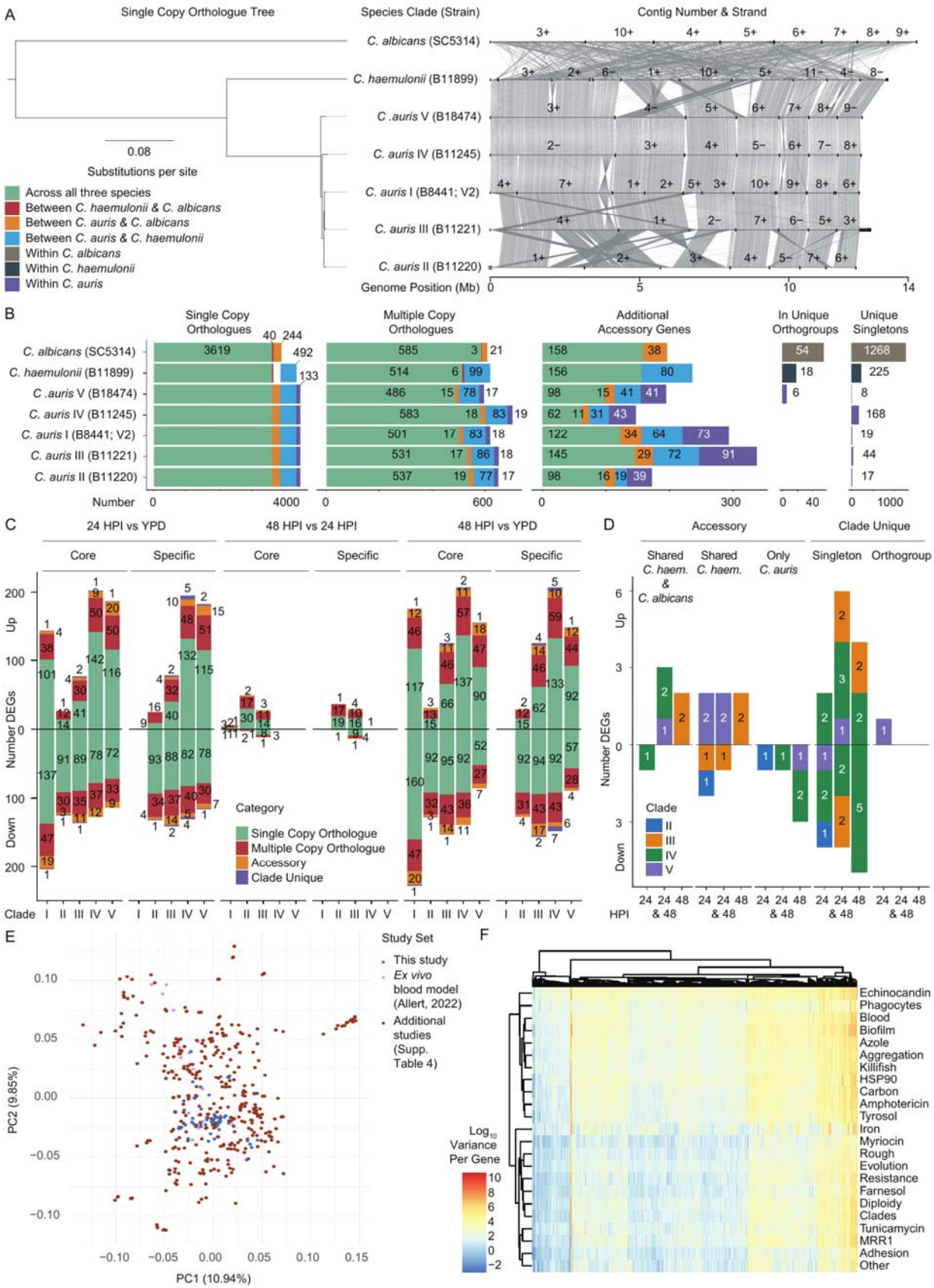
A
Single Copy Orthologue Tree
Species Clade (Strain)
Contig Number & Strand
C. albicans (SC5314)
C. haemulonii (B11899)
C .auris V (B18474)
C. auris IV (B11245)
C. auris I (B8441; V2)
C. auris III (B11221)
C. auris II (B11220)
Genome Position (Mb)
0.08
Substitutions per site
Across all three species
Between C. haemulonii & C. albicans
Between C. auris & C. albicans
Between C. auris & C. haemulonii
Within C. albicans
Within C. haemulonii
Within C. auris
B
Single Copy Orthologues
Multiple Copy Orthologues
Additional Accessory Genes
In Unique Orthogroups
Unique Singletons
Number
C
24 HPI vs YPD
48 HPI vs 24 HPI
48 HPI vs YPD
Core
Specific
Up
Down
Number DEGs
Clade
Category
Single Copy Orthologue
Multiple Copy Orthologue
Accessory
Clade Unique
D
Accessory
Clade Unique
Shared C. haem. & C. albicans
Shared C. haem.
Only C. auris
Singleton
Orthogroup
Clade
II
III
IV
V
HPI
E
Study Set
This study
Ex vivo blood model (Allert, 2022)
Additional studies (Supp. Table 4)
PC1 (10.94%)
PC2 (9.85%)
F
Log10 Variance Per Gene
Echinocandin
Phagocytes
Blood
Biofilm
Azole
Aggregation
Killifish
HSP90
Carbon
Amphotericin
Tyrosol
Iron
Myriocin
Rough
Evolution
Resistance
Farnesol
Diploidy
Clades
Tunicamycin
MRR1
Adhesion
Other

1364

Supplementary Figure 3. Contextualising differential gene expression across orthogroups and broder RNA-seq datasets. (A) Single copy orthologue phylogeny and Synima/Orthofinder synteny plot of reference genomes for *C. albicans, C. haemulonii* and the five clades of *C. auris* used in this study. Despite many orthologues, there is little synteny with *C. albicans*; prominent translocations and inversions are seen between *C. haemulonii* and *C. auris*, and for clade II. **(B)** Counts are shown for orthologues contained within and between species, whether single copy or multiple copy, with additional counts for accessory genomes. Clade V is the only *C. auris* clade with a single orthogroup, containing six genes, while clade IV has the highest number of apparently unique genes that were not assigned to any orthogroup. **(C)** Differential gene expression for *in vivo vs in vitro* comparisons, comparing numbers of DEGs identified when using a single core reference genome (B8441, clade I) or a clade-specific reference genome for each individual clade. **(D)** Differential expression of specific genes not present in core reference genome. **(E)** RNA-seq meta-analysis. 36 public datasets were identified for *C. auris* transcriptome expression and assessed for variance by PCA dimensionality reduction of normalised expression of single copy orthologues, indicating AK dataset clusters similarly to experiments using an *ex vivo* blood model and other experiments. **(F)** Hierarchical clustering of per-gene variance, calculated for all B8441 core genes for each study, demonstrating similar clustering and profile of within-experiment variance per gene.

Down
Up
24 HPI
48 HPI
24 vs YPD
48 vs 24
48 vs YPD
GO Biol. Process
GO:0034219: carbohydrate transmembrane transport
GO:0008643: carbohydrate transport
GO:0097080: plasma membrane selenite transport
GO:0006811: monoatomic ion transport
GO:0035433: acetate transmembrane transport
GO:0019740: nitrogen utilization
GO:0072488: ammonium transmembrane transport
GO:0006544: glycine metabolic process
GO:0000027: ribosomal large subunit assembly
GO:0006412: translation
GO:0002181: cytoplasmic translation
GO:0006825: copper ion transport
GO:0051156: glucose 6-phosphate metabolic process
GO:0046835: carbohydrate phosphorylation
GO:0008202: steroid metabolic process
GO:0006629: lipid metabolic process
GO:0006044: N-acetylglucosamine metabolic process
GO:0005975: carbohydrate metabolic process
GO:0006260: DNA replication
GO:0006694: steroid biosynthetic process
GO:0044088: regulation of vacuole organization
GO:0009251: glucan catabolic process
GO:0030174: regulation of DNA-templated DNA replication initiation
GO:0051515: positive regulation of monopolar cell growth
GO:0061091: regulation of phospholipid translocation
GO:0035672: oligopeptide transmembrane transport
GO:1903710: spermine transmembrane transport
GO:0071555: cell wall organization
GO:0000103: sulfate assimilation
GO:0030447: filamentous growth
GO Cell. Compart.
GO:0016020: membrane
GO:0005575: cellular_component
GO:0000324: fungal-type vacuole
GO:0031410: cytoplasmic vesicle
GO:0005886: plasma membrane
GO:0005737: cytoplasm
GO:0005829: cytosol
GO:0005634: nucleus
GO:0005960: glycine cleavage complex
GO:1990904: ribonucleoprotein complex
GO:0005840: ribosome
GO:0071944: cell periphery
GO:0005656: nuclear pre-replicative complex
GO:0042555: MCM complex
GO:0071162: CMG complex
GO:0031966: mitochondrial membrane
GO:0009277: fungal-type cell wall
GO:0005576: extracellular region
GO Mol. Function
GO:0015578: mannose transmembrane transporter activity
GO:0005315: inorganic phosphate transmembrane transporter activity
GO:0016705: oxidoreductase activity (paired donors)
GO:0097079: selenite:proton symporter activity
GO:0004497: monooxygenase activity
GO:0015343: siderophore-iron transmembrane transporter activity
GO:0015123: acetate transmembrane transporter activity
GO:0022857: transmembrane transporter activity
GO:0000293: ferric-chelate reductase activity
GO:0003674: molecular_function
GO:0008519: ammonium transmembrane transporter activity
GO:0000166: nucleotide binding
GO:0030527: structural constituent of chromatin
GO:0046982: protein heterodimerization activity
GO:0016740: transferase activity
GO:0019843: rRNA binding
GO:0003723: RNA binding
GO:0016773: phosphotransferase activity, alcohol group as acceptor
GO:0005536: glucose binding
GO:0019158: mannokinase activity
GO:0003697: single-stranded DNA binding
GO:0016491: oxidoreductase activity
GO:0017116: single-stranded DNA helicase activity
GO:0003688: DNA replication origin binding
GO:0020037: heme binding
GO:0000297: spermine transmembrane transporter activity
GO:0035673: oligopeptide transmembrane transporter activity
GO:0004190: aspartic-type endopeptidase activity
KEGG
K08139: HXT; MFS transporter, SP family, sugar:H+ symporter
K08197: ARN; MFS transporter, SIT family, siderophore-iron:H+ symporter
K08192: DAL5; MFS transporter, ACS family, DAL5 transporter family protein
K07034: K07034; uncharacterized protein
K11253: H3; histone H3
K11251: H2A; histone H2A
K00844: HK; hexokinase [EC:2.7.1.1]
K06005: SAP; candidapepsin [EC:3.4.23.24]
PFAM
PF15789.9: Hyr1: Hyphally regulated cell wall GPI-anchored protein 1
PF11765.12: Hyphal_reg_CWP: Hyphally regulated cell wall protein N-terminal
PF01425.25: Amidase: Amidase
PF00083.28: Sugar_tr: Sugar (and other) transporter
PF00067.26: p450: Cytochrome P450
PF07738.17: Sad1_UNC: Sad1 / UNC-like C-terminal
PF03583.18: LIP: Secretory lipase
PF12988.11: TraQ_transposon: TraQ conjugal transfer protein
PF15580.10: Imm53: Immunity protein 53
PF05730.15: CFEM: CFEM domain
PF08030.16: NAD_binding_6: Ferric reductase NAD binding domain
PF01184.23: Gpr1_Fun34_YaaH: GPR1/FUN34/yaaH family
PF01794.23: Ferric_reduct: Ferric reductase like transmembrane component
PF08022.16: FAD_binding_8: FAD-binding domain
PF07690.20: MFS_1: Major Facilitator Superfamily
PF00125.28: Histone: Core histone H2A/H2B/H3/H4
PF00428.23: Ribosomal_60s: 60s Acidic ribosomal protein
PF16211.9: Histone_H2A_C: C-terminus of histone H2A
PF06609.17: TRI12: Fungal trichothecene efflux pump (TRI12)
PF00349.25: Hexokinase_1: Hexokinase
PF03727.20: Hexokinase_2: Hexokinase
PF00493.27: MCM: MCM P-loop domain
PF01078.25: Mg_chelatase: Magnesium chelatase, subunit ChlI
PF14551.10: MCM_N: MCM N-terminal domain
PF17207.7: MCM_OB: MCM OB domain
PF17855.5: MCM_lid: MCM AAA-lid domain
PF03169.19: OPT: OPT oligopeptide transporter protein
PF00026.27: Asp: Eukaryotic aspartyl protease
Other
Accessory
NetGPI: GPI-Anchored
DeepTMM Predicted TM-domain(s)
SignalP5: SP(Sec/SPI)
FDR
0.00025
0.00050
0.00075
Ratio
0.2
0.4
0.6
Mean log-fold change
10
5
0
-5
Clade Comparison

1385

Supplementary Figure 4. *C. auris* Gene Set, Pathway and Domain Enrichment: Transcripts from *C. auris* reference genomes for each clade were annotated for Gene Ontology (GO) terms using DIAMOND2GO, Kyoto Encycopaedia of Genes and Genome pathways using BLASTKoala, PFAM domains using HMMScan, transemembrane domains with DeepTMHMM, GPI-anchored domains with NetGPI, SignalP domains with SignalP5, and membership within the accessory genome using Synima/Orthofinder. For each set of up-regulated or down-regulated genes in each comparison, Fisher's exact test was used with Benjamini-Hochberg (BH) correction for multiple testing for each set, with a false discovery rate (FDR) cut-off of 0.001. Mean log-fold change and ratio of genes in that set was calculated for genes in each set possessing each feature.

Supplementary Figure 5. *C. auris* Mating-Type Locus Gene Expression: (A) Transcripts (fragments per kilobase per million, FPKM) for orthogroups aligned to the same reference genome (left-hand panels) and clade-specific reference genomes (right-hand panels), indicating similar transcript levels between clades for e.g. *PIKA*, *OBPA* and *PAP1* non-mating genes when aligned to clade-specific reference genomes. **(B)** Comparing individual transcript levels for each orthogroup in more *vs* less virulent clades *via* Wilcoxon signed-rank test with Bonferroni correction to minimise false positives, demonstrating that only down-regulation of *THI4* (at 24 HPI), *MRD1* (at both time-points), and up-regulation of *PGA30* and *PIKA* were significantly different.

Significance levels are as follows: * p <= 0.05, ** <= 0.01, *** <= 0.001, **** <= 0.0001, ***** <= 0.00001.

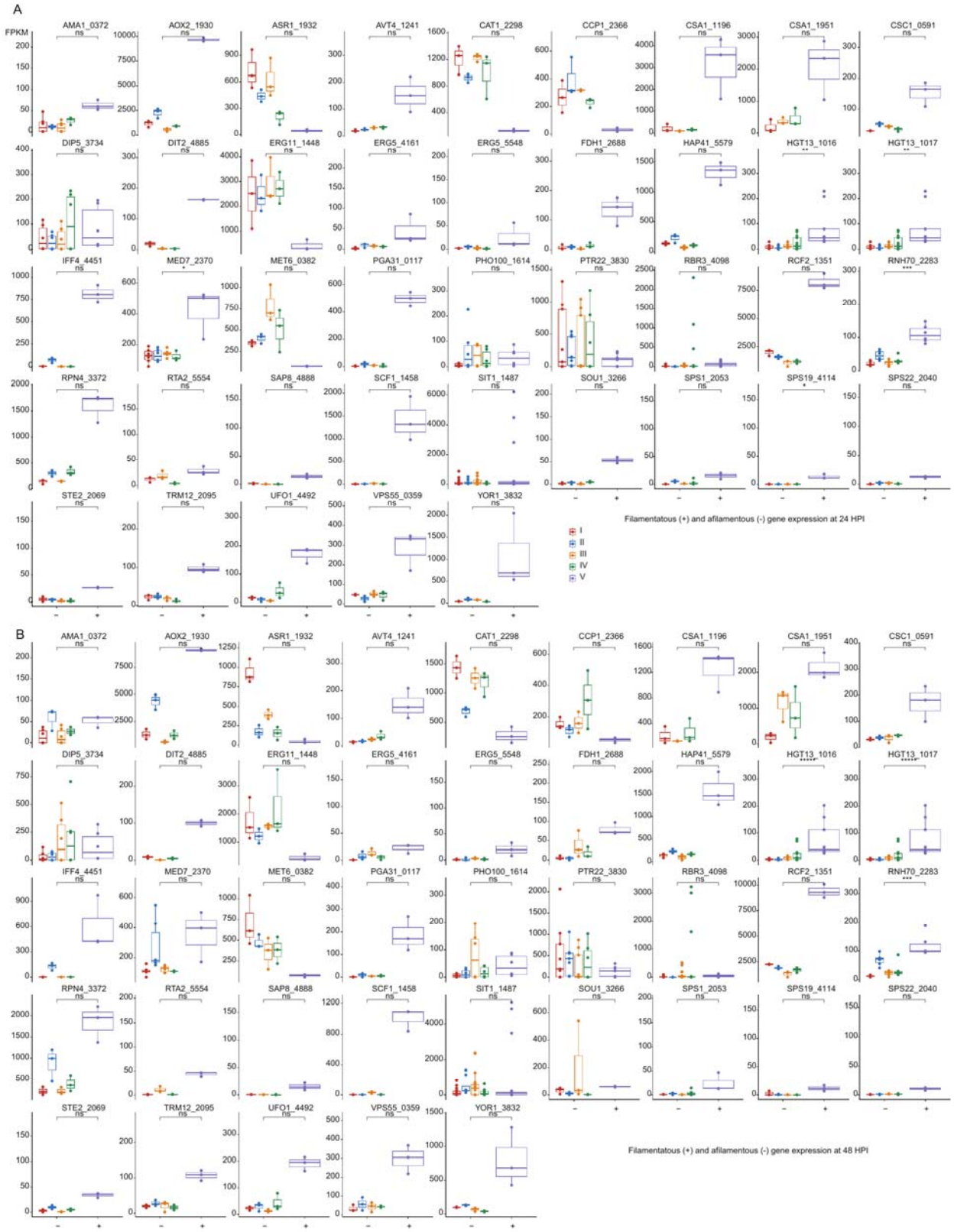
A
FPKM
AMA1_0372
AOX2_1930
ASR1_1932
AVT4_1241
CAT1_2298
CCP1_2366
CSA1_1196
CSA1_1951
CSC1_0591
DIP5_3734
DIT2_4885
ERG11_1448
ERG5_4161
ERG5_5548
FDH1_2688
HAP41_5579
HGT13_1016
HGT13_1017
IFF4_4451
MED7_2370
MET6_0382
PGA31_0117
PHO100_1614
PTR22_3830
RBR3_4098
RCF2_1351
RNH70_2283
RPN4_3372
RTA2_5554
SAP8_4888
SCF1_1458
SIT1_1487
SOU1_3266
SPS1_2053
SPS19_4114
SPS22_2040
STE2_2069
TRM12_2095
UFO1_4492
VPS55_0359
YOR1_3832
Filamentatous (+) and afilamentous (-) gene expression at 24 HPI
I
II
III
IV
V
B
Filamentatous (+) and afilamentous (-) gene expression at 48 HPI

1409

Supplementary Figure 6: (A-B) *Comparing individual transcript levels for each orthogroup in filamentous clade V vs all other clades via Wilcoxon signed-rank test with Bonferroni correction to minimise false positives, demonstrating at 24 HPI* ***(A)*** *and 48 HPI* ***(B)****, excluding any genes that were assigned to be 'hypothetical proteins' only, up-regulation of two HGT13 orthologues and RNH70 were significantly different at both time-points, with up-regulation of MED7 and SPS19 at 24 HPI. Significance levels are as follows: Significance levels are as follows: * p <= 0.05, ** <= 0.01, *** <= 0.001, **** <= 0.0001, ***** <= 0.00001.*

Supplementary Tables

Supplementary Table 1. Clade-Representative *Candida auris* Strains Used In This Study: Representative strain for each major clade of *C. auris* used in the study, with notes on human disease source, country of discovery, and date of isolation. Mortality statistics are given in terms of absolute numbers of embryos over biological triplicate experiments. Additional significance testing is also noted for pairwise comparisons by Log-Rank test with Benjamini-Hochberg (BH) correction.

Supplementary Table 2: Differentially Expressed Genes in *A. dispar* Microinjection: All differentially expressed genes (DEGs) for *A. dispar* for (upper rows) sham injection *vs* no injection and (lower rows) *C. auris* injection *vs* sham injection. Gene IDs and descriptions follow annotations by Bonzi *et al.*[85]; log-fold change and -$\log_{10}$(false discovery rate) are calculated across all clades as a mean value for *C. auris* injection. Significant DEGs for each set of embryos injected with each clade are given (1 = significant, 0 = not significant), and the total number of clades where DEGs where significant is also given.

Supplementary Table 3. Differentially Expressed Genes in *C. auris* Infection: (A) Combined set of differentially expressed genes (DEGs) expressed by five clades during

infection Each set of DEGs expressed *in vivo vs in vitro* for five clades was combined, resulting in a set of genes that were specific to *C. auris* infection at these timepoints. **(B)** Combined set of DEGs between more virulent and less virulent clades: Each set of DEGs between clades I & IV (more virulent) and II & III (less virulent) was compared at 24 HPI and 48 HPI, resulting in a combined set expressed in infection. **(C)** Combined DEG Sets: between filamentous clade V and all other clades: Each set of DEGs between clade V and all each clades I-IV was compared at 24 HPI and 48 HPI, resulting in a combined set expressed in infection, excluding those significant during growth in YPD broth where clade V was not observed to filament. **(D)** Accessory genes not found in clade I reference genome: DEGs without orthologues in the clade I reference were identified and annotated.

Supplementary Table 4. Publicly available RNA-seq Data on 16th April 2024: A systematic re-analysis of RNA expression across NCBI-available datasets for *C. auris* gene expression, categorised by research theme for analysis (**Fig. S1D-E**).